NATIONAL AERONAUTICS AND SPACE ADMINISTRATION

Technical Memorandum 33-726

Approach Guidance for Outer Planet Pioneer Missions

Antal K. Bejczy

JET PROPULSION LABORATORY
CALIFORNIA INSTITUTE OF TECHNOLOGY
PASADENA, CALIFORNIA

May 1, 1975

NATIONAL AERONAUTICS AND SPACE ADMINISTRATION

Technical Memorandum 33-726

Approach Guidance for Outer Planet Pioneer Missions

Antal K. Bejczy

JET PROPULSION LABORATORY
CALIFORNIA INSTITUTE OF TECHNOLOGY
PASADENA, CALIFORNIA

May 1, 1975

PREFACE

The work described in this report was performed by the Guidance and Control Division of the Jet Propulsion Laboratory for the NASA/Ames Advanced Space Projects Office, and was first presented at the XXVth Congress of the International Astronautical Federation.

CONTENTS

I. Introduction 1

II. Mission Requirements and Approach Guidance 2

III. Sensor and Application Concepts 2

IV. Measurements and Measurables 5

V. Pioneer Entry Probe Missions to Uranus 5

A. Saturn-Uranus Mission, Saturn Encounter 6

B. Saturn-Uranus Mission, Uranus Approach 9

C. Jupiter-Uranus Mission, Uranus Encounter 11

VI. Spacecraft Attitude and Approach Guidance Measurements 13

VII. Discussion of Results 16

Acknowledgement 18

References 18

Appendix: Measurement of Long Term Spin Axis Stability of Pioneer 10 20

TABLES

1. Targeting Accuracy Requirements and Capabilities . . . 2

2. Mission Data Applied in the Analysis 5

FIGURES

1. V-Slit Star Mapper Configuration 3

2. V-Slit Star Mapper Application Concept 3

3. V-Slit Star Mapper Operation Principle 4

4. Approach Guidance Measurement Process 4

5. Definition of Viewing Parameters 6

6. Saturn-Uranus Mission, Saturn Flyby 6

PRECEDING PAGE BLANK NOT FILMED

7. Saturn-Uranus Mission, Saturn Flyby; Saturn and Outer Ring Angular Diameter 6

8. Saturn-Uranus Mission, Saturn Flyby; Satellite Viewing Parameters 7

9. Saturn-Uranus Mission, Saturn Flyby; Satellite Viewing Parameters 7

10. Saturn-Uranus Mission, Saturn Flyby; Satellite Viewing Cone Angle 8

11. Saturn-Uranus Mission, Saturn Flyby; Satellite Viewing Geometry 8

12. Saturn-Uranus Mission, Saturn Flyby; Tracking Titan Against Star Background, VM < 4 9

13. Saturn-Uranus Mission, Saturn Flyby; Tracking Titan Against Star Background, VM < 5 10

14. Saturn-Uranus Mission, Uranus Approach 11

15. Saturn-Uranus Mission, Uranus Approach; Uranus Angular Diameter 11

16. Saturn-Uranus Mission, Uranus Approach; Satellite Angular Diameter 12

17. Saturn-Uranus Mission, Uranus Approach; Satellite Phase Angle 12

18. Saturn-Uranus Mission, Uranus Approach; Satellite Viewing Parameters 12

19. Saturn-Uranus Mission, Uranus Approach; Satellite Viewing Parameters 13

20. Saturn-Uranus Mission, Uranus Approach; Satellite Viewing Parameters 13

21. Saturn-Uranus Mission, Uranus Approach; Satellite Viewing Cone Angle 13

22. Saturn-Uranus Mission, Uranus Approach; Satellite Viewing Geometry 14

23. Saturn-Uranus Mission, Uranus Approach; Tracking Titania Against Star Background, VM < 4 14

24. Saturn-Uranus Mission, Uranus Approach; Tracking Titania Against Star Background, VM < 5 15

25. Jupiter-Uranus Mission, Uranus Approach; Satellite Phase Angle 15

26. Jupiter-Uranus Mission, Uranus Approach; Satellite Viewing Cone Angle 16

27. Jupiter-Uranus Mission, Uranus Approach; Tracking Titania Against Star Background, VM < 4 16

28. Jupiter-Uranus Mission, Uranus Approach; Tracking Titania Against Star Background, VM < 5 17

A-1. Jupiter Viewing Parameters Relative to Pioneer 10 20

A-2. Scanning Jupiter from Pioneer 10 with the IPP in the Imaging Mode in May/June 1974 20

A-3. Scanning Jupiter in June 1974; Output Samples from the IPP in the Imaging Mode 21

ABSTRACT

This report deals with onboard optical approach guidance measurements for spin-stabilized Pioneer-type spacecraft to improve spacecraft targeting accuracy and onboard fuel economy by supplementing earth-based radio navigation. Approach guidance measurement accuracy requirements vs advanced Pioneer mission requirements are outlined. The sensor investigated in this report is a V-slit star tracker. The application concept and operation principle of the sensor are discussed within the context of approach guidance measurements and measurables. It is also shown that the accuracy of onboard optical approach guidance measurements is inherently coupled to the stability characteristics of the spacecraft spin axis. Extensive sets of geometrical and physical measurement parameters are presented for Pioneer entry probe missions to Uranus via Jupiter or Saturn flyby. The measurement parameters are related to the Uranus encounter phase of both missions as well as to the Saturn flyby phase of the Saturn-Uranus mission. The impact of the measurement parameters on both sensor instrumentation and measurement system design is discussed. The need for sensing extended objects is shown. The report concludes with the indication of the feasibility of implementing an onboard approach guidance measurement system for Pioneer-type spacecraft. The Appendix briefly describes two Pioneer 10 onboard measurement experiments performed in May-June 1974 by using the imaging photopolarimeter locked on Jupiter in the imaging mode to study the spin axis stability of Pioneer-type spacecraft at a fine (~5-10 arc-sec) resolution level.

APPROACH GUIDANCE FOR OUTER PLANET PIONEER MISSIONS

Antal K. Bejczy
Member of the Technical Staff
Jet Propulsion Laboratory
California Institute of Technology
Pasadena, California 91103

I. Introduction

In the last few years, a great deal of interest has developed for in-situ investigation of the atmospheres of the outer planets. Scientific reasoning indicates that these atmospheres may represent a storehouse of information on the evolution of the solar system. The Outer Solar System Science Advisory Group of NASA has recommended that a series of Pioneer-type missions to be launched to Saturn and Uranus in 1979-1980 be studied in greater detail. (Ref. 1.) In particular, the study of the following two missions has been recommended: 1979 Pioneer Entry Probe to Saturn and 1980 Pioneer Entry Probe to Uranus via Saturn Flyby or, alternatively, via Jupiter Flyby. Pursuing these recommendations, mission planning studies have been undertaken for Pioneer-type Saturn/Uranus Atmospheric Entry Probe Missions. (Ref. 2.)

Joining the mission planning studies, this paper deals with an overall parametric system analysis of the use of an optical approach guidance measurement system onboard a Pioneer-type spin-stabilized spacecraft for outer planet missions. For a number of advanced Pioneer missions, a "radio plus optical" approach guidance technique has been proposed in previous studies (Refs. 3, 4, 5) to satisfy both terminal accuracy requirements and onboard fuel economy. Expected terminal accuracy improvements and onboard fuel saving resulting from a "radio plus optical" guidance and navigation have been quantitatively outlined in Ref. 6 for three different outer planet Pioneer missions. For a three-axis stabilized Mariner-type spacecraft, the feasibility of using an onboard TV camera for precise terminal guidance and navigation has already been demonstrated at JPL (Refs. 7, 8).

The approach guidance measurement system investigated in this paper employs a V-slit electro-optical "star pipper" (Refs. 3, 4, 5). It can be a separate instrument or, eventually, combined with an onboard "imaging" system (Ref. 9). The sensor concept is similar to that which has successfully been applied to attitude determination of some of the earth-orbiting spin-stabilized satellites as, for instance, the OSO-7 satellite (Ref. 10). The sensor system contains a small telescope (3 deg field-of-view) with a V-slit reticle at the image plane, a photomultiplier, and appropriate data processing electronics. The slit width of the V-shaped reticle is 20 arcsec. The optical axis of the sensor can be gimballed relative to the spacecraft spin axis. Due to the spacecraft spin, the sensor field-of-view scans an annular strip of the celestial sphere. As the images of detectable stars and the target (satellites of a planet or the planet itself) pass the V-slit, the photodetector generates a sequence of pulse pairs. The timing of the pulse signatures can be used to determine the angular position of the target relative to identifiable reference stars as seen from the spacecraft.

This study considers the use of optical measurements of the satellites of Saturn and Uranus against the star background. Measuring the angular position of the satellites against the star background as the satellites revolve about the planet, the barycenter of the system can be determined which is the sought data for approach guidance. (Refs. 11 and 12.) To satisfy approach guidance accuracy requirements, the precision needed in the determination of the relative spacecraft-target direction is 100 to 150 μrad, which in turn requires 40 to 60 μrad sensor data accuracy.

Beyond the physical characteristics of the V-slit sensor instrumentation, two factors critically influence the required measurement accuracy: measurement geometry and spacecraft attitude. Both factors are evaluated in depth with respect to two alternative outer planet Pioneer missions: Saturn-Uranus and Jupiter-Uranus atmospheric entry probe missions with departure from Earth in November/December 1980. A comprehensive set of measurement geometry parameters are presented for both the Saturn flyby and Uranus approach mission phases. Available data on attitude performance of Pioneer and other spin-stabilized spacecrafts (Refs. 10, 13, and 14) are employed in the analysis. A brief, preliminary evaluation of long-term attitude stability measurements of Pioneer 10 by using the onboard Imaging Photopolarimeter with the 100 arcsec square aperture locked on Jupiter for 8 to 28 hours in May/June 1974 is presented in the Appendix. Reference is also made to a recent V-slit sensor breadboard test. (Ref. 15.)

In conclusion, a trade-off is presented for an approach guidance measurement system for advanced outer planet Pioneer missions using a V-slit sensor. The major conclusions are: (1) At Saturn flyby, viewing some of the medium period satellites can provide the best measurement results. (2) At Uranus approach, viewing the planet itself may offer the most advantageous measurements if an early bus-probe separation is required. (3) In all cases, the final measurement accuracy strongly depends on both the data format transmitted to Earth and the applied data interpretation techniques using appropriate models of sensor performance and of spacecraft attitude dynamics.

II. Mission Requirements and Approach Guidance

Exploration of distant solar system objects (comets, asteroids, outer planets, and their satellites) by space probes requires probe delivery accuracies which are beyond the present earth-based radio navigation capabilities. Earth-based radio navigation for targeting a spacecraft relative to a solar system object essentially utilizes a time-dependent vector difference formed between the heliocentric state vector of the target object and that of the spacecraft. The accuracy of the resultant spacecraft-target difference vector is basically limited by the accuracy at which the target ephemeris data are known since the uncertainty in the target ephemeris data are much larger than the error in the best estimate of the spacecraft trajectory obtainable from radio tracking.

The best terminal error using only earth-based radio navigation is listed in the first column of Table 1 for several advanced missions under current study. The terminal accuracy required to complete the missions with the desired success is listed in the second column of Table 1. As seen, the terminal error obtainable from "radio-only" navigation is several times larger than the desired delivery error. To achieve the desired delivery accuracies by "radio-only" navigation would require target ephemeris accuracy equivalent to 0.1 arcsec or better resolution in earth-based target observations. (Depending on the particular distant solar system object, the best ephemeris data presently available are equivalent to 0.3-0.5 arcsec resolution.)

Table 1. Targeting Accuracy Requirements and Capabilities

MISSION		RADIO-ONLY NAVIGATION ERROR 10^3 km	REQUIRED TERMINAL ACCURACY 10^3 km	REQUIRED DIRECTION MEASUREMENT ACCURACY μrad	REQUIRED SENSOR DATA ACCURACY μrad
MULTIPLE PLANET FLYBY		2-10	1	100-150*	40-60*
MULTIPLE ASTEROID		2-8	0.2-0.5		
COMET FLYBY		5-15	0.2-0.5		
SATURN-URANUS OR JUPITER-URANUS ENTRY PROBE	AT JUPITER	0.8	0.5-1.0		
	AT SATURN	2-3	0.4-0.6		
	AT URANUS	8-10	1.5-2.0		

*TAKING ACCOUNT OF ACQUISITION RANGE AND OF MIDCOURSE ΔV ALLOWANCE

Substantial terminal accuracy improvement can be achieved, however, by the application of a spacecraft-based approach guidance measurement system capable of determining the celestial direction of the target mass center relative to the spacecraft. In conjunction with earth-based radio tracking of the spacecraft, the spacecraft-based measurements of the celestial coordinates of the target contain the information needed to derive a more accurate target-centered position of the spacecraft so that the spacecraft position relative to the target will be known to an accuracy reflected as an 0.1 arcsec or better target ephemeris error.

The basic goal of an approach guidance measurement system is to obtain spacecraft-based measurements of the spacecraft-target direction vector referenced to celestial coordinates. The method of obtaining this information is that of measuring the angular separation between the target and known bright stars. If the target is a planet, then the measurements can be of the angular position of the planet's satellite(s), and from these measurements the angular position of the target planet will be deduced. The error associated with an indirect determination of the planet's angular position can be less than the error related to a direct measurement of the planet's angular position relative to known bright stars when the planet is seen as a largely extended object from the spacecraft. The measurement of angular separation between planetary satellites and known bright stars involves only images of point light sources if the spacecraft is at a sufficiently large distance from the satellite(s).

The accuracy requirements for a spacecraft-based approach guidance measurement system should be viewed together with the onboard fuel allowances for trajectory correction maneuvers. In a first approximation, the miss distance error ΔD corresponding to a given angular measurement error $\Delta\alpha$ is directly proportional to the spacecraft-target distance so that $\Delta D \sim R\Delta\alpha$. On the other hand, the equivalent ΔV velocity maneuver required to correct the miss distance error is inversely proportional to the spacecraft-target distance so that $\Delta V \sim VD/R$. Consequently, for a given onboard fuel allowance for trajectory correction there is an equivalent approach guidance direction measurement accuracy requirement, or vice versa. For a given approach guidance measurement system accuracy, the best practical strategy is to perform the measurement and trajectory correction process iteratively by removing a large portion of the miss distance at an early date when the ΔV requirements are small, and correcting the residual error at a later date when the measurement accuracy is improved.

Taking account of the considerations above, the third column of Table 1 lists the accuracy required from the approach guidance measurement system to satisfy mission requirements. The fourth column of Table 1 is specifically related to the signal accuracy of a V-slit sensor considered for use on a Pioneer-type spin-stabilized spacecraft for approach guidance measurements. It is noted that the basic quantity measured by a V-slit sensor is time or time difference and not direct angular separation between objects which can be provided by TV frame measurements. In the case of a V-slit "star pipper", the spacecraft-target angular direction is derived from timing measurements.

III. Sensor and Application Concepts

Consider a small telescope with a V-slit reticle at the image plane mounted on a suitable place of the spinning spacecraft. If the telescope having a θ degree field of view is pointed by ϕ degree away from the direction of the spin axis, it will under ideal conditions inscribe a circular path in the sky and sweep a θ degree wide annular strip in the sky as the spacecraft rotates around the spin axis. Detectable stars and the target object appearing within the scanned annular strip of the sky will

generate a sequence of pulse (or wave) pairs as their images pass the slit of the V-shaped reticle which defines the instantaneous field of view. Accurate timing measurements of the pulses (or the center of the waves) can be used for a precision determination of both the inertial orientation of the spacecraft spin axis and the angular position of the planetary satellite relative to detectable known stars. In particular, the mean time and the separation time of each pulse (or wave) pair provide the sensed object's clock and cone angles, respectively, defined relative to the spacecraft spin axis. V-slit type sensors have been successfully applied to attitude determination of several spin-stabilized earth-orbiting satellites. (See, for instance, Refs. 10, 13, and 14.)

The V-slit sensor under consideration in this study has 20 arcsec slit width and 3 degree field-of-view. The narrow slit width aids the detection accuracy of signals coming from point light sources. The 3 degree field-of-view is a trade-off value to assure a sufficient number of detectable stars, brighter than 4 Visual Magnitude (VM), within various scanned annular strips of the sky. The sweep cone of the sensor can be controlled by mechanically gimballing the telescope relative to the spacecraft spin axis.

The sensor configuration is shown in Fig. 1. As seen, the V-slit star mapper is a relatively simple sensor. It consists of five major components: objective lens, V-slit reticle, field lens, photodetector, and data processor. The electro-optical design considerations for a particular V-slit sensor configuration suitable for approach guidance measurements can be found in Ref. 15.

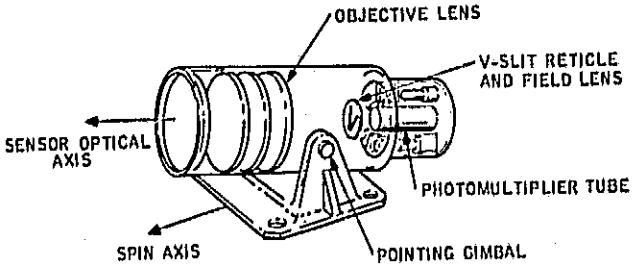

Fig. 1. V-Slit Star Mapper Configuration

The V-slit sensor application concept for approach guidance measurements is shown in Fig. 2. The sensor operation principle is shown in Fig. 3. The upper parts of Fig. 3 show the operating polar reference frame fixed to the spacecraft. As seen in the lower part of Fig. 3, the field-of-view has two dimensions: an angular width in the scan direction, and an angular length in the direction normal to the scan direction. The area of sky scanned per revolution depends on the angular length of the detector, and the detector angular width determines the dwell time of a signal at a given spin rate. The rotation of the spacecraft will produce high signal-to-noise ratio pulses as images of stars and the satellite cross the reticle slits. Each object generates a pulse pair. With reference to the lower part of Fig. 3, the pulses at t_1 and t_3 are generated by objects "a" and "b", respectively, when they cross the clock angle (vertical) reference

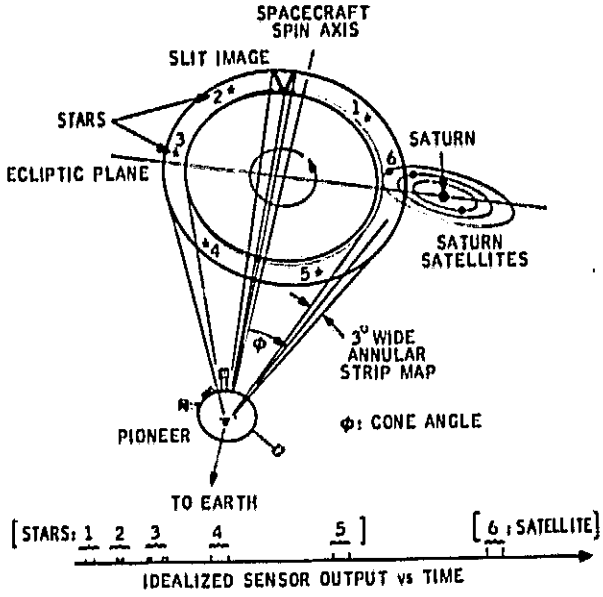

Fig. 2. V-Slit Star Mapper Application Concept

slit. Hence, t_3-t_1 is proportional to the differential clock angle between objects "a" and "b". On the other hand, the pulses at t_2 and t_4 are generated by objects "a" and "b", respectively, when they cross the cone angle (slanted) reference slit. Hence, t_2-t_1 and t_4-t_3 are proportional to the differential cone angle of objects "a" and "b", **respectively, in the sensor field-of-view.** It is seen that an accurate determination of angular position becomes now a problem of accurate measurement of time differences.

Regarding accuracy in time measurements, of specific interest are the signal detection techniques applicable to implementing time interval measurements. The simplest technique is the indication of a fixed threshold crossing. This technique, however, introduces error in the clock angle measurements since the threshold will trigger at different times for different input amplitudes. The input amplitude is a function of star or satellite light intensity. Assuming that the same amplitude is generated at each slit, the cone angle measurements will not be influenced by this error. The error in the clock angle measurements can be decreased in several ways. Encoding the peak amplitude following a threshold crossing would be perhaps the most advantageous technique for three reasons. First, the center of the pulse can be computed by knowing the crossing time, peak amplitude, and filter response. Second, signal wave forms resulting from the sensing of extended objects can be interpreted more accurately by knowing the peak amplitude at each point. Third, the measurement of the peak amplitude of star pulses will greatly aid the identification of stars which is an all important element in the approach guidance measurement process.

The approach guidance measurement process by using a V-slit star mapper onboard a spin-stabilized spacecraft is summarized in a functional block diagram in Fig. 4. Though one successful measurement can improve the accuracy of the

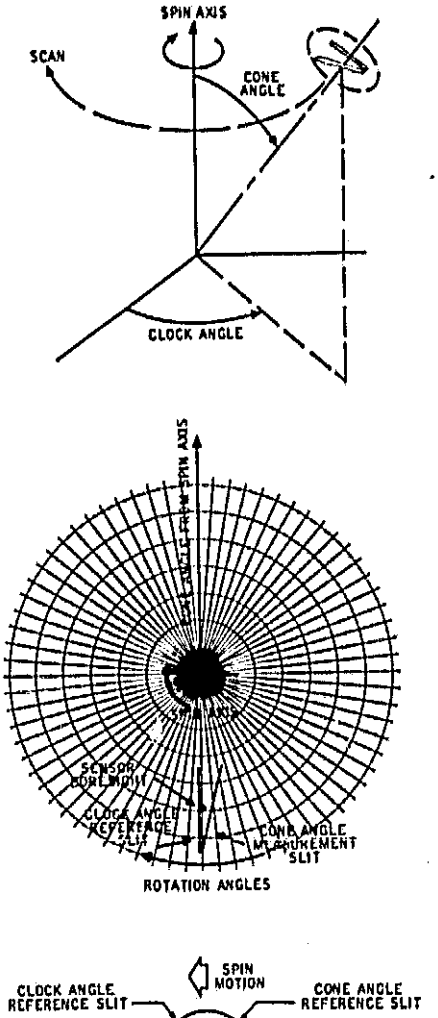

Fig. 3. V-Slit Star Mapper Operation Principle

spacecraft-target direction vector, the measurement and computational process should be repeated over the entire orbital period of the sensed satellite in order to take full advantage of the approach guidance measurement system as shown in Ref. 6. Of course, if the planetary satellite itself is the mission target, then the satellite's ephemeris is the sought final approach guidance data which will

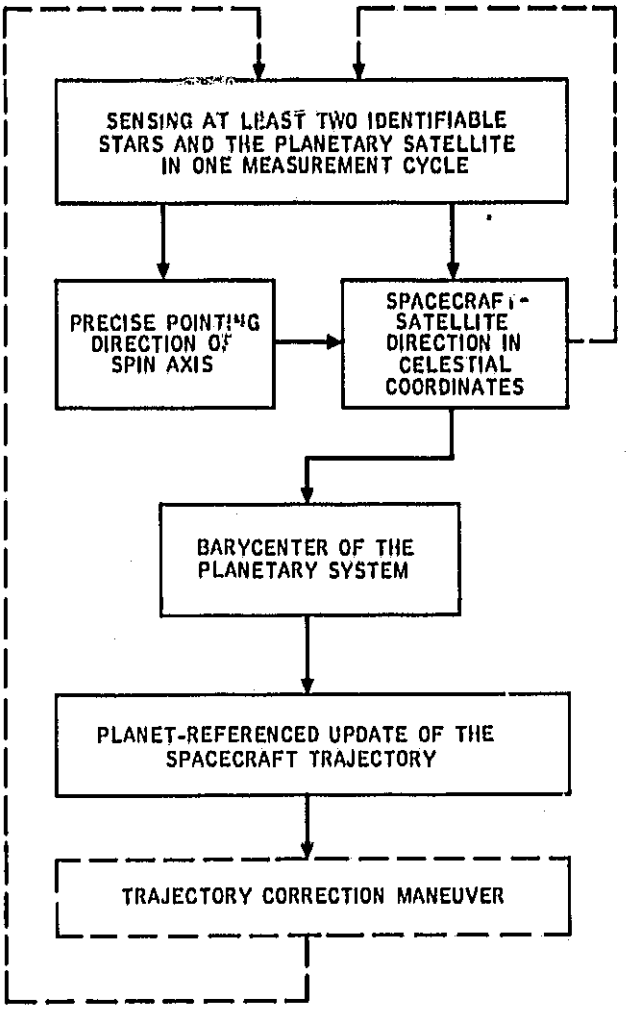

Fig. 4. Approach Guidance Measurement Process

be considerably improved by a measurement process repeated over the entire orbital period of the satellite. It is also noted that more than two identifiable stars within the scanned annulus of the sky and repeated scans over the same field of view can improve approach guidance measurement accuracy within the limits of the fine structure stability of the spin axis.

Recently, a breadboard V-slit star mapper was tested at TRW to determine the feasibility of such a sensor to provide the signal accuracy required for approach guidance measurements onboard a Pioneer-type spinning spacecraft. (Ref. 15.) The breadboard sensor had the following main characteristics. Objective lens: 300 mm f.l., f/3.5. Field lens: 17.8 mm diameter, 31 mm f.l. Photomultiplier: EMR 541E-01-14 S-20 Photocathode. Reticle geometry: 15.88 mm (3.03 deg) slit length, 25.4 μm (17.4 arcsec) slit width, 25.9 deg slant angle for V-shape. Threshold detection: 2 KHz BW.

The test results were encouraging. For a 40 deg cone angle and with 5 rpm, the error in the clock and cone angle measurements of a point light source equivalent to 4.9 VM was in the range

of 10-15 and 15-25 arcsec, respectively. Several techniques have been suggested to improve the first test results.

IV. Measurements and Measurables

The primary data sought in the approach guidance measurement process is the angular position of planetary satellites relative to known reference stars. Thus, the approach guidance sensor can functionally be defined as an electro-optical instrument capable of measuring natural satellite positions against known background stars as seen from the spacecraft. Since the spacecraft under consideration is a spin-stabilized vehicle, its natural rotation in the inertial space can conveniently be utilized in a star scanner sensor instrumentation.

The basic measurable is the light radiation from stars and the target converted into electrical signals by the detector. For sensor design and successful performance, the following measurement parameters are of specific interest. (1) Definition of the satellite(s) which will be tracked by the V-slit sensor. (2) Apparent size and brightness of the tracked satellite as seen from the spacecraft. (3) Apparent separation of the tracked satellite(s) from the target planet as seen from the spacecraft. (4) The cone angle of the sensor optical axis required to view the satellite(s) from the spinning spacecraft. (5) Available star background for a required set of viewing cone angles.

Onboard optical approach guidance measurements by a V-slit sensor are inherently coupled to the attitude motion of the spacecraft since the measurements are relative spacecraft-target directions expressed in celestial coordinates, and the sensor's inertial orientation at any given time is a function of the spacecraft attitude. Thus, the accuracy of optical approach guidance measurements by a V-slit sensor is limited by the accuracy to which the attitude of the spin-stabilized spacecraft is known at the time when the spacecraft-target direction measurements are being taken. Consequently, the inherent coupling of the onboard optical approach guidance measurements leads to the problem of precision modelling the attitude motion of a Pioneer-type spin-stabilized spacecraft in order to extract the maximum information from the measurements.

A precision performance of approach guidance measurements in real flight assumes also several flight calibration procedures to compensate for non-random sensor errors. The analysis of such calibration techniques is beyond the scope of this paper.

V. Pioneer Entry Probe Missions to Uranus

Regarding delivery accuracy, the most critical advanced outer planet Pioneer missions under current study are the 1980 Pioneer Entry Probe Missions to Uranus via Saturn or Jupiter Flyby. It has been shown (Ref. 6) that an onboard optical approach guidance measurement system is essential for probe delivery at Uranus because of the combined effect of three factors: early bus/probe separation date (about 20 days before encounter), narrow entry corridor for probe delivery at Uranus, and the pathologically large ephemeris error of Uranus (see Table 1). In particular, it was found that, for the selected probe entry point location, the dispersion of the probe trajectory in the impact plane must be kept under 2000 km.

In this section, approach guidance measurement geometry parameters are presented for both the Saturn-Uranus and Jupiter-Uranus missions. For the Saturn-Uranus mission, the measurement geometry has been computed for both the Saturn flyby and Uranus approach phases. For the Jupiter-Uranus mission, the measurement geometry has been computed only for the Uranus approach phase since it has been shown (Ref. 6) that the guidance accuracy obtainable by "radio only" navigation measurements would be satisfactory at the Jupiter flyby phase of a Jupiter-Uranus mission.

The physical parameters of Uranus and Saturn and their satellites needed for the computations have been taken from Refs. 16 and 17. The mission data used in the computations are those which have been determined in Ref. 2 and listed in Table 2.

Table 2. Mission Data Applied in the Analysis

	SATURN-URANUS MISSION	JUPITER-URANUS MISSION
1. EARTH DEPARTURE	NOVEMBER 25, 1980	DECEMBER 9, 1980
2. SATURN ENCOUNTER	JANUARY 5, 1984	
3. APPROACH ASYMPTOTIC VECTOR AT SATURN		
a) V_∞ (km/sec)	10.44	
b) ECLIPTIC LATITUDE (deg)	0.627	
c) ECLIPTIC LONGITUDE (deg)	188.43	
4. AIM POINT FOR SATURN ENCOUNTER		
a) R: PERIAPSIS RADIUS (km)	164872	
b) ϕ_T: AIM ANGLE**(deg)	-2.08	
5. URANUS ENCOUNTER	NOVEMBER 9, 1987	APRIL 2, 1986
6. APPROACH ASYMPTOTE VECTOR AT URANUS		
a) V_∞ (km/sec)	15.77	14.75
b) ECLIPTIC LATITUDE (deg)	+2.0026	+0.42108
c) ECLIPTIC LONGITUDE (deg)	276.9914	245.7927
7. AIM POINT FOR URANUS ENCOUNTER*		
a) R: PERIAPSIS RADIUS (km)	35648.41	14799.34
b) ϕ_T: AIM ANGLE**(deg)	276.977	32.9414

*PRIOR TO PROBE SEPARATION FROM THE BUS IN THE BUS DEFLECTED MISSION MODE

**MEASURED FROM THE T-VEC FOR PI THE B-PLANE SO THAT THE T-VECTOR IS IN THE ECLIPTIC PLANE

The measurement geometry parameters at Uranus approach have been computed for the time period starting from 80 days before encounter (E-80) and ending at 10 days before encounter (E-10). The contemplated primary goal for both alternative missions is the successful delivery of an entry probe to Uranus. As seen from Table 2, both missions considered in the computations are in the bus deflected mode (Ref. 2*). According to

*In the bus deflected mode, the spacecraft and probe are initially targeted at the appropriate entry location and, at some point inside the sphere of influence of the planet, the probe is separated and the spacecraft is deflected to the appropriate nonimpacting trajectory.

previous studies (Refs. 2, 5, and 6), entry probe separation from the bus would take place approximately 20 days before Uranus encounter. Optical approach guidance measurements, therefore, should take place at a time period preceding the probe separation from the bus.

The definition of some of the measurement geometry parameters is explained in Fig. 5. The definition of the other geometry parameters (apparent angular size of the object and apparent angular separation of satellite from planet limb) is obvious. As seen in Fig. 5, it is assumed that the spacecraft spin axis is always pointing toward the Earth like the spin axis of the presently operational Pioneer 10 and 11 spacecraft.

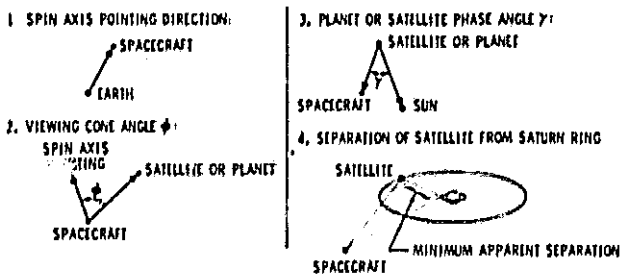

Fig. 5. Definition of Viewing Parameters

The apparent brightness m_v of the planet and the satellites is computed according to the known formula:

$$m_v = m_e + [\quad \log R + \log r] + F(\gamma) + f(\beta)$$

where

m_e: normalized visual magnitude (VM)

R: distance from sun to target

r: distance from spacecraft to target

$F(\gamma)$: phase angle correction

$f(\beta)$: applied only to Saturn, correcting for the apparent ring inclination β relative to the line of sight.

The values of m_e for Saturn, Uranus and their satellites used in the calculations are taken from Refs. 16 and 18.

A. Saturn-Uranus Mission, Saturn Encounter

In the viewing parameter calculations, four Saturn satellites have been considered: Hyperion, Titan, Rhea, Dione. The primary target candidates for approach guidance measurements are Titan and Rhea. Hyperion is too faint and Dione is too close to the planet.

Figs. 6 and 7 show the essential apparent viewing parameter of Saturn. Though Saturn is not a viewing target for navigational fixes, its brightness and angular diameter, together with the outer ring's angular diameter, should be taken into account in the satellite scanning process, because of possible stray light interference.

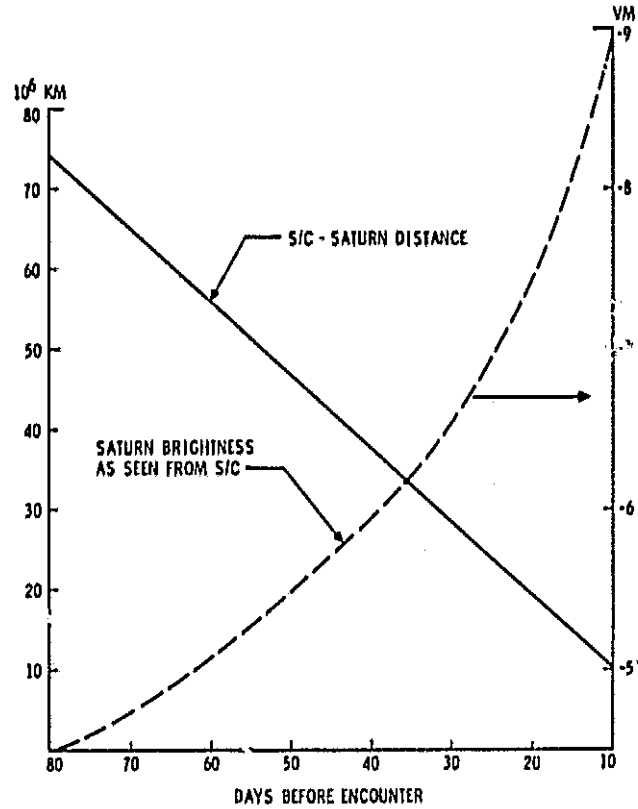

Fig. 6. Saturn-Uranus Mission, Saturn Flyby

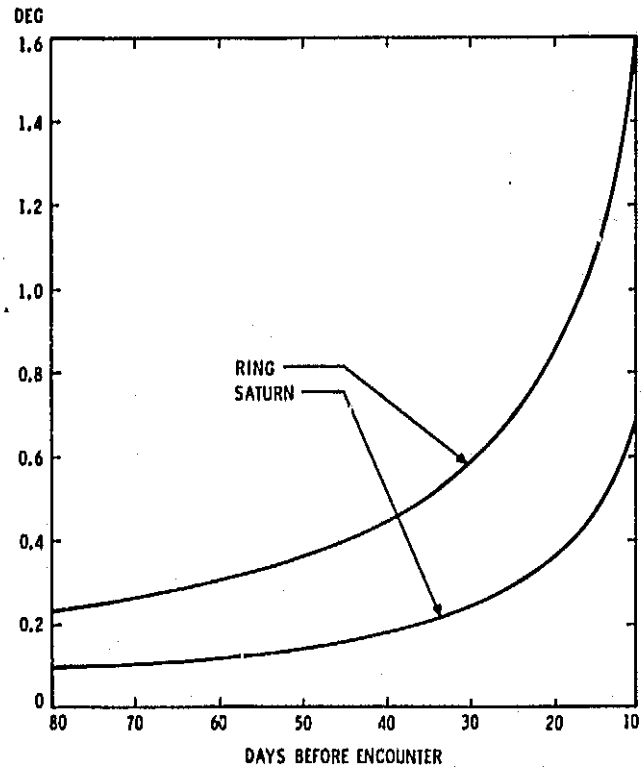

Fig. 7. Saturn-Uranus Mission, Saturn Flyby; Saturn and Outer Ring Angular Diameter

The basic viewing parameters for Titan and Rhea are shown in Figs. 8 through 10. As seen in Fig. 8, the apparent angular diameter of Titan is near to or greater than 20 arcsec in the time period between E-80 and E10 days. Therefore, Titan should be considered as an extended and not a point-like object. Even Rhea becomes an extended object at E-20 day as seen in Fig. 8. The apparent phase angle variations for Titan and Rhea are also shown in Fig. 8. When the sensed target object appears as an extended body in the field of view of the V-slit sensors, the target's phase angle should be taken into account for interpreting the target's signature.

As seen in Fig. 9, Titan is a bright object, and can be visible for a 4 VM sensitivity sensor earlier than E-100 day. However, the maximum apparent angular separation of Titan from the Saturn ring reaches 1 deg only at E-60 day as seen in Fig. 9. Tentatively, it is assumed that the apparent angular separation of the scanned satellite from the ring (or from the planet limb) should be at least 1 deg to avoid stray light interference from the much brighter planet.

Fig. 9 shows that Rhea will appear as a 4 VM object at E-65 day, but its maximum apparent angular separation from the Saturn ring reaches 1 deg only at E-25 day. However, the orbital period of Rhea is less than 5 days so that at least two complete orbits can be measured during the time

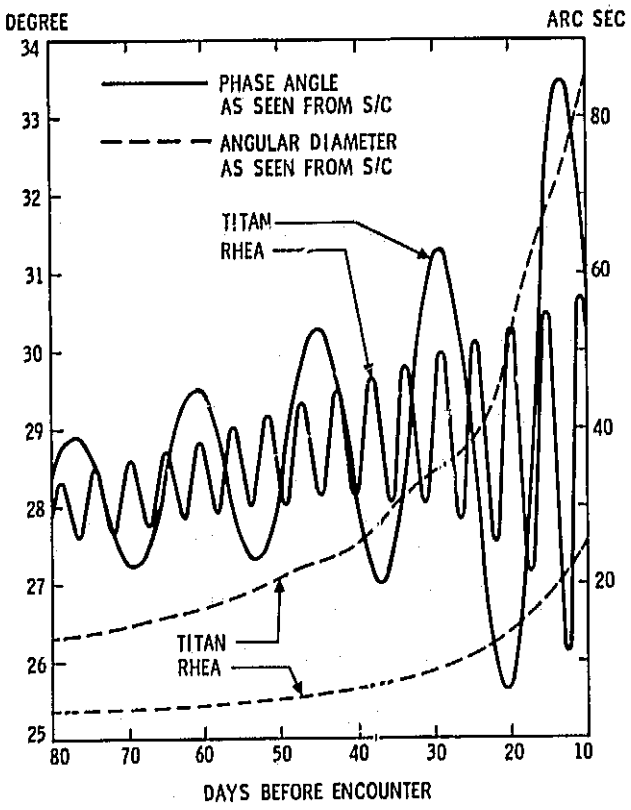

Fig. 8. Saturn-Uranus Mission, Saturn Flyby; Satellite Viewing Parameters

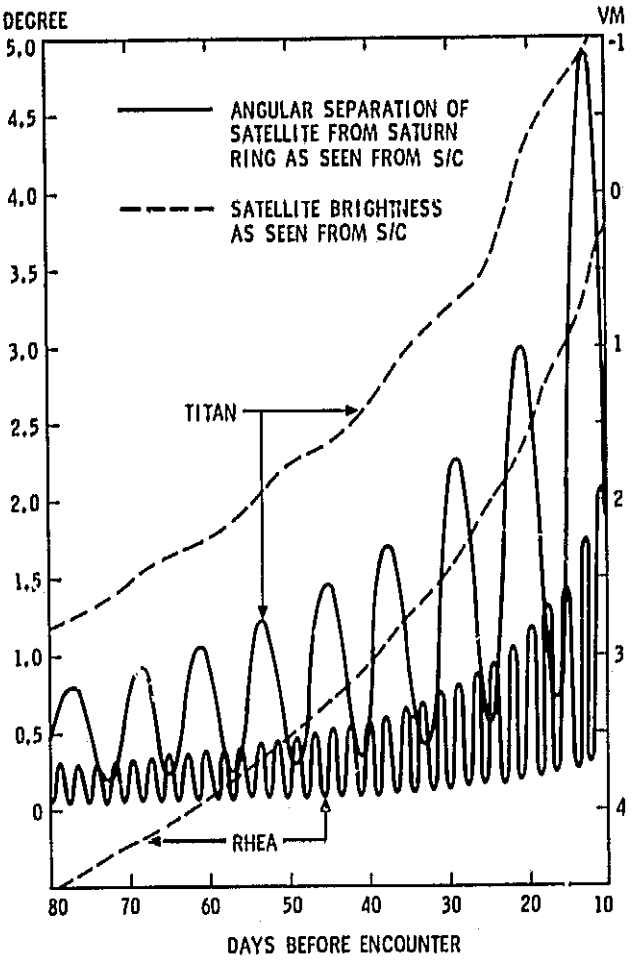

Fig. 9. Saturn-Uranus Mission, Saturn Flyby; Satellite Viewing Parameters

period between E-25 and E-15 days. Note that the time difference between three successive peak points of the apparent angular separation curves corresponds to the orbital period of the satellite.

The viewing cone angle variations for the four Saturn satellites are shown in Fig. 10 which also displays the Saturn viewing cone angle for reference. In general, the useful satellite viewing cone angle must satisfy the following constraint:

$$\phi_{satellite} \gtrless \phi_{planet} \pm (0.5\beta + \Delta\xi)$$

where

β: apparent angular diameter of the planet (or ring)

$\Delta\xi$: required minimum angular separation of the sensor's field of view from the planet limb (or from the ring).

Note that, in general, the maximum and minimum points of the satellite viewing cone angle

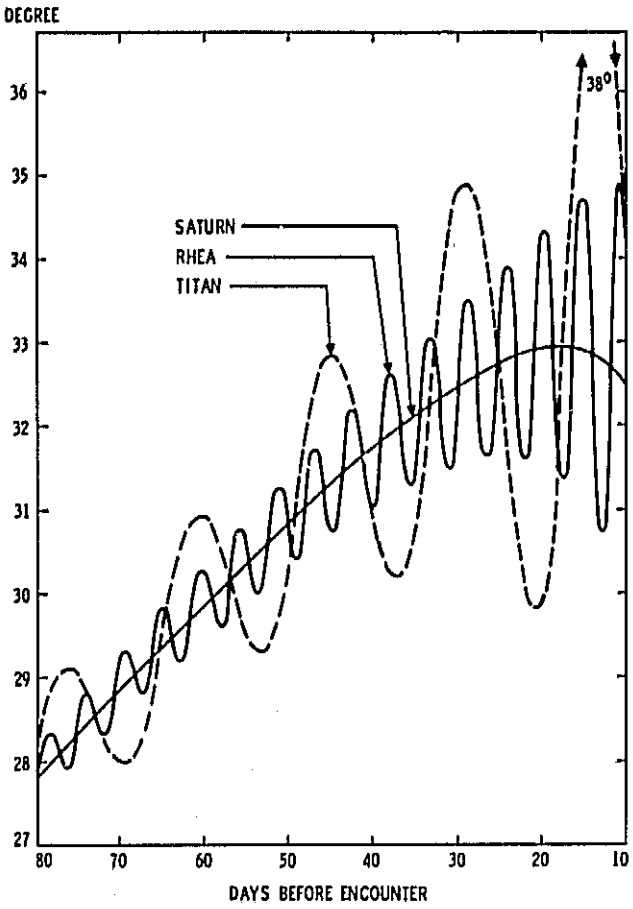

Fig. 10. Saturn-Uranus Mission, Saturn Flyby; Satellite Viewing Cone Angle

curves correspond to the situations when the satellite appears farthest to the left or farthest to the right (or vice versa) relative to the planet as seen from the spacecraft. As seen in Fig. 10, the useful satellite viewing cone angles range from 30 to 35 degrees which can be considered satisfactory for approach guidance measurements.

Fig. 11 shows the satellite viewing geometry for a 3 deg field of view V-slit scanner in the actual angular dimensions scaled to the E-25 day conditions. The apparent angular diameter of Saturn and its outer ring has also the proper scale. Of course, the 20 arcsec slit width and the apparent angular diameter of the satellites are out of the scale and only serve illustrative purposes. The location of the satellites in their orbit is also illustrative only. But the angular extension of the orbit is in proper scale.

The scanned star background with stars down to 4 and 5 VM is shown in Figs. 12 and 13, respectively. The figures also show the path of the spin axis pointing in the time period between E-80 and E-10 days. For convenience, a continuous time history has been plotted for the spin axis pointing. Actually, the spin axis would be precessed only periodically and stepwise to keep the high gain antenna within ~ 0.3 deg of the earth line-of-sight. The apparent orbit of Titan from E-37 to E-21 day is also shown in the figures together with the

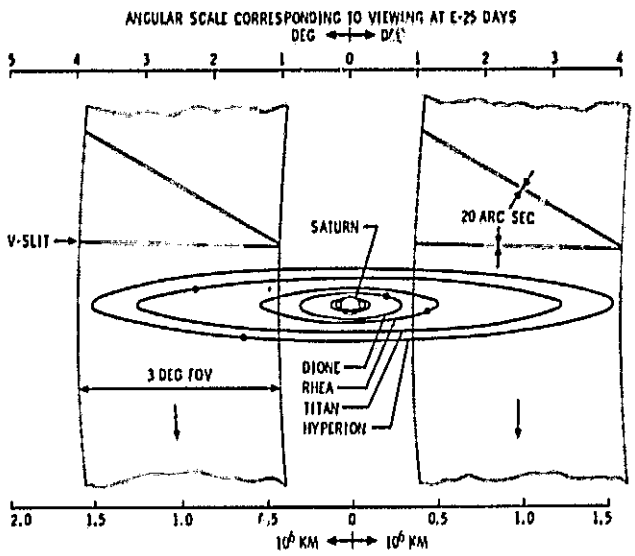

Fig. 11. Saturn-Uranus Mission, Saturn Flyby; Satellite Viewing Geometry

apparent location of Saturn. The 3 deg wide annular scan of the V-slit sensor shown in Figs. 12 and 13 is centered at the spin axis pointing at E-30 day. The apparent location of Titan at E-30 day is also shown in the figures. Since the star background is shown in a Cartesian frame, the scanned annular strip appears as a distorted circular ring in the figures. It is noted that, from spherical trigonometry, the celestial coordinates of a small circle in the celestial sphere must satisfy the following relation:

$$\cos\phi = \cos(\alpha' - \alpha)\cos\delta'\cos\delta + \sin\delta'\sin\delta$$

where

ϕ: cone angle (angular radius) of the small circle

δ, α: declination and right ascension of the center of the small circle

δ', α': declination and right ascension of the locus of the small circle.

The distorted circles in Figs. 23 and 24 are drawn for $\delta = -13.26$ deg, $\alpha = 220.08$ deg, $\phi = 33.7$ and 36.7 deg, and satisfy the relation quoted above.

As seen in Fig. 12, the 3 deg wide annular strip contains, in addition to Titan, 1 star brighter than 2.5 VM and 6 stars with brightness between 2.5 and 4 VM. The total 85 deg by 85 deg celestial background contains 73 stars brighter than 4 VM, or 220 stars brighter than 5 VM. That is, increasing the sensitivity of the V-slit star mapper from 4 VM to 5 VM objects would add 147 detectable reference stars to that particular celestial background. It is seen from Fig. 12 that a 4 VM sensitivity V-slit star mapper would be sufficient for approach guidance measurements at Saturn. Note also in Fig. 12 how evenly the detectable stars are distributed within the annular strip. This favorable condition also prevails for 3 deg annular strips with 27 to 30 deg cone angles.

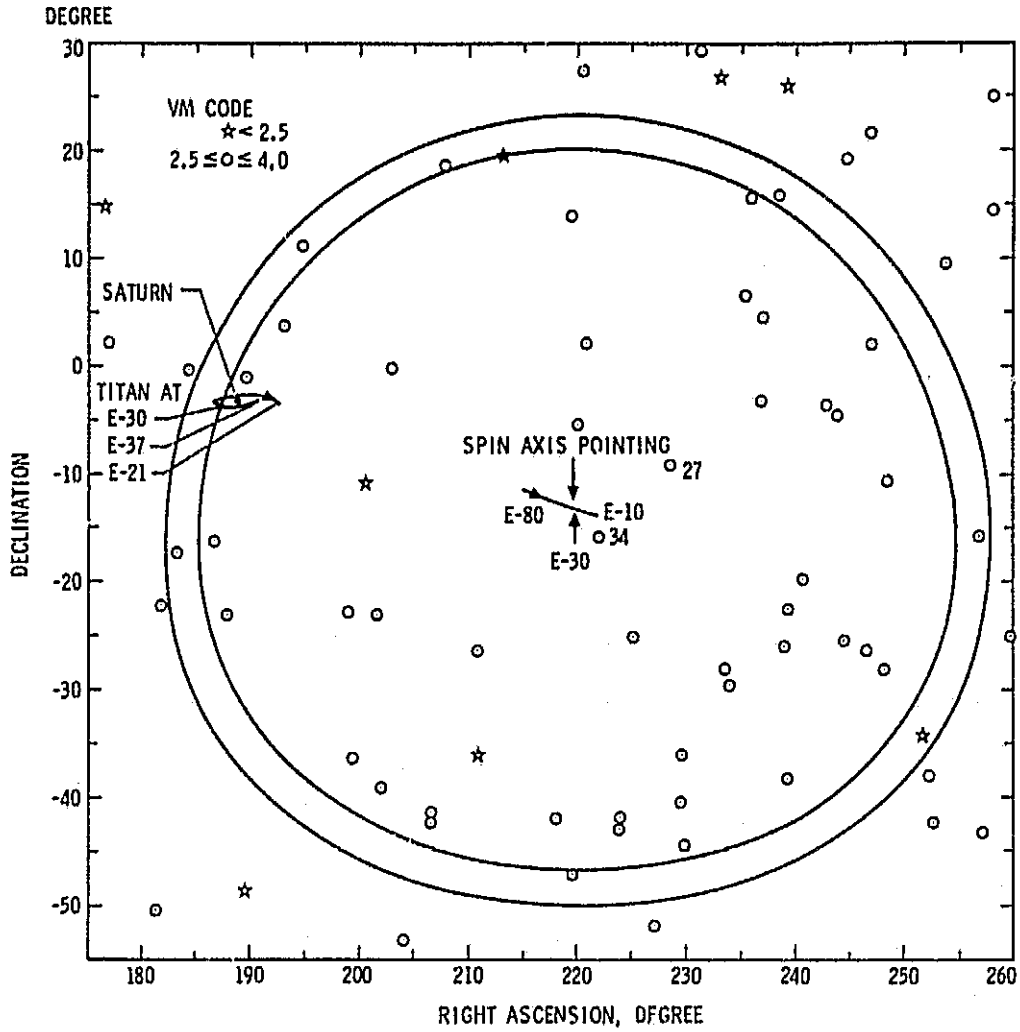

Fig. 12. Saturn-Uranus Mission, Saturn Flyby; Tracking Titan Against Star Background, VM < 4

B. Saturn-Uranus Mission, Uranus Approach

In the viewing parameter calculations, four Uranus satellites have been considered. Though the primary target candidate for approach guidance measurements is Titania, the viewing geometry of the other satellites may also have an impact on the measurements for reasons to be discussed later.

Figs. 14 and 15 show the essential apparent viewing parameters for Uranus. It is worth noting in these figures that the angular diameter and brightness of Uranus as seen from the spacecraft during the time period from E-60 to E-40 are in the range of 100-150 arcsec and minus 1.8 to minus 2.7 VM, respectively. Fig. 14 also shows the spacecraft-Uranus distance for the corresponding time period.

The basic viewing parameters for four Uranus satellites are shown in Figs. 16 through 21. As seen in Fig. 16, all Uranus satellites can be considered as point objects prior to E-15 day. Approximately at E-10 day, however, the apparent angular diameter of Titania, Oberon and Ariel becomes 20 arcsec. But the phase angle is favorable as seen in Fig. 17. (Almost full phase.)

The satellite brightness curves shown in Figs. 18 through 20 should be taken with some reservation. Comparing the earth-observed brightness data for the Uranus satellites as quoted in Refs. 16 and 18, it is safe to state that the data have at least ±0.3 VM uncertainty. It is noted that the angular separations of satellites from the planet surface shown in Figs. 18 and 19 are mean values. Small periodic variations in the values of the apparent angular separation are omitted from these figures.

Fig. 20 gives synoptic displays of the relevant "close-up" data for viewing Titania and Oberon during the time period between E-30 to E-16 days.

It is seen from Fig. 18 that Umbriel is an unsuitable observation object for a 4-th VM sensitivity terminal guidance optical sensor for the time period prior to E-20 days. Even a sensitivity increase of the V-slit sensor to 6-th VM objects would not make Umbriel a suitable observation target. Though Umbriel could be detected with a 6-th VM sensitivity optical sensor at E-30 days, the apparent angular separation of Umbriel from the Uranus surface during the time period from E-30 to E-20 days is so small (0.35-0.5 deg)

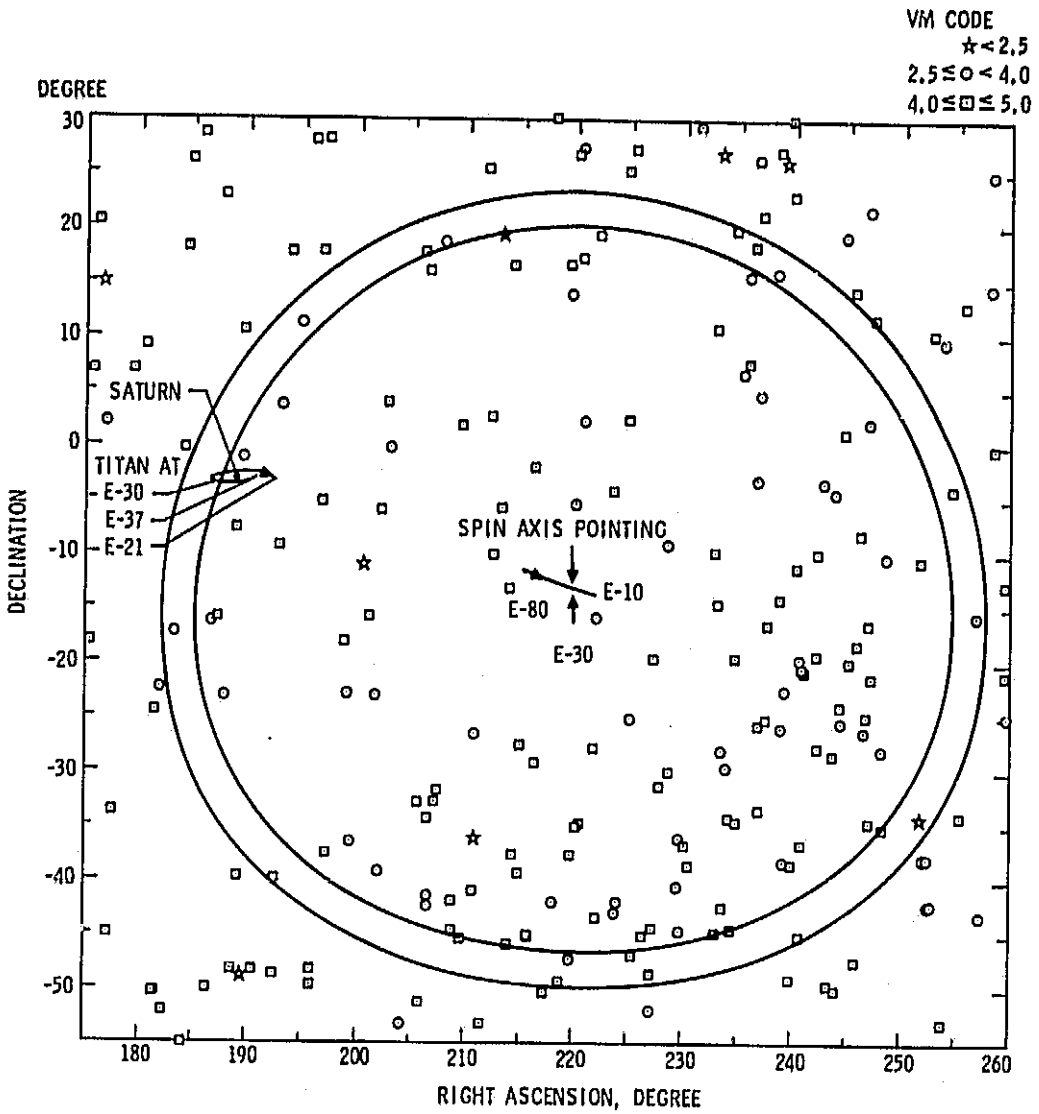

Fig. 13. Saturn-Uranus Mission, Saturn Flyby; Tracking Titan Against Star Background, VM < 5

that Umbriel should be ruled out as a potential observation object for approach guidance.

Figs. 18 and 19 show that Ariel, Titania and Oberon would be 4-th VM objects as seen from the spacecraft approximately at E-20 day. As pointed out in Ref. 6, at least one complete satellite orbit observation is required for satisfactory approach guidance calculations. This requirement dictates that the sensitivity of the onboard V-slit guidance sensor should be increased at least to 5-th VM objects since the orbital period of Titania and Oberon is 8.7 and 13.5 days, respectively, and the probe-bus separation takes place at E-20 day. As seen in Figs. 18 through 20, with a 5-th VM sensitivity V-slit sensor Titania and Oberon can be detected approximately at E-35 and E-32 days, respectively, so that at least one observation of their complete orbit can be performed by the onboard sensor prior to E-20 day. Note, however, that the apparent angular separation of Titania and Oberon from the Uranus surface as seen from the spacecraft at E-35 and E-32 days is approximately only 0.5-0.8 degree.

Among the five Uranus satellites, Titania and Oberon seem to be the most suitable observation objects for approach guidance measurements provided that the sensitivity of the V-slit sensor is increased from the presently contemplated 4-VM level to the 5 VM level. As to the question of selection preference for observing Titania or Oberon for approach guidance measurements, Titania is the preferred satellite due to its shorter orbital period (8.7 days) and somewhat brighter appearance.

Though Titania and/or Oberon seem the most suitable observation objects for approach guidance measurements, Ariel may also represent an interesting alternative; with a 5 VM sensitivity V-slit sensor, Ariel could be detected from the spacecraft at E-30 day. (See Fig. 18.) These detection days would provide the possibility of observing 3 to 4 complete orbits of Ariel prior to the E-20 day probe-bus separation date, since the orbital period of Ariel is 2.5 days. Note, however, that the apparent angular separation of Ariel from the Uranus surface as seen from the spacecraft at E-30 to E-25 days is approximately only 0.4-0.5 degree.

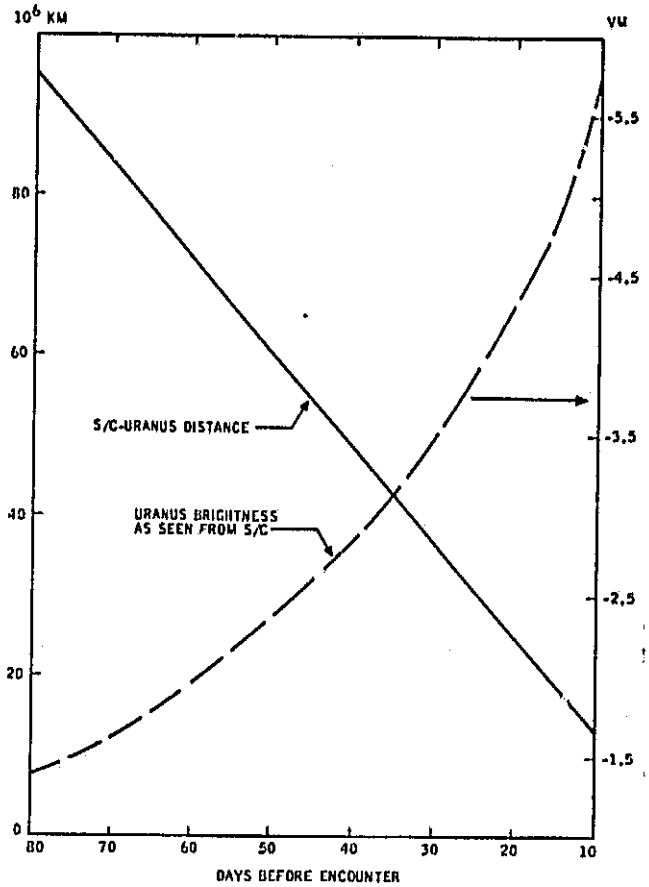

Fig. 14. Saturn-Uranus Mission, Uranus Approach

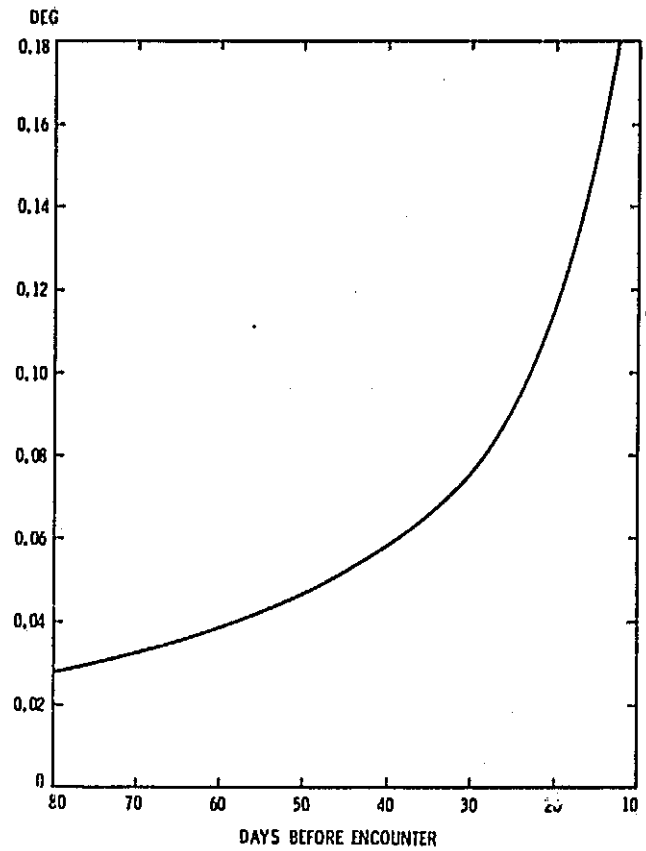

Fig. 15. Saturn-Uranus Mission, Uranus Approach; Uranus Angular Diameter

The viewing cone angle variations for four Uranus satellites are shown in Fig. 21 for the time period between E-40 and E-16 days. For reference, the figures also show the Uranus viewing cone angle. As seen, the useful satellite viewing cone angles are quite narrow. (About 13 and 15 deg, respectively.)

Fig. 22 at the end of this subsection shows the satellite viewing geometry for a 3 deg field of view V-slit scanner in the actual angular dimensions scaled to the E-25 day conditions. The apparent angular diameter of Uranus has also the proper scale in the figure. But the 20 arcsec slit width and the satellite angular diameters are out of the scale of Fig. 22.

The scanned star background with stars down to 4 and 5 VM is shown in Figs. 23 and 24, respectively. The figures also show the path of the spin axis pointing in the time period between E-80 and E-10 days. The apparent orbit of Titania from E-32 to E-21 day is also shown in the figures together with the apparent location of Uranus. The 3 deg wide annular scan of the V-slit sensor shown in Figs. 23 and 24 is centered at the spin axis pointing at E-28 day with coordinates δ = -23.39 deg, α = 262.08 deg; the cone angle is ϕ = 14 and 11 deg. The apparent location of Titania at E-28 day is also shown in the figures. The construction of the distorted small circles in a Cartesian frame has been explained previously.

As seen in Fig. 23, the 3 deg wide annular strip contains, in addition to Titania, 2 stars brighter than 2.5 VM and 3 stars with brightness between 2.5 and 4 VM. The total 40 deg by 40 deg celestial background contains 25 stars brighter than 4 VM, or 72 stars brighter than 5 VM. Increasing the sensitivity of the V-slit sensor to 5 VM would also provide a more favorable star distribution within the scanned annular strip of the sky.

C. Jupiter-Uranus Mission, Uranus Encounter

The apparent viewing parameters for Uranus and its satellites would practically be identical to the corresponding parameter values shown previously for the Saturn-Uranus mission, (see Figs. 14 through 20), except the apparent phase angle which now becomes even smaller (about 4.5 deg, see Fig. 25). The evaluation of satellite viewing conditions outlined in the previous subsection for the Saturn-Uranus mission could be repeated here with identical conclusions for the Jupiter-Uranus mission.

Regarding the viewing cone angles, however, there is a significant difference between the Jupiter-Uranus and Saturn-Uranus missions. Comparing Figs. 26 and 21, it is seen that the viewing cone angle for Uranus and its satellites becomes even narrower during the Jupiter-Uranus mission. (About 7 deg, that is, half of the viewing

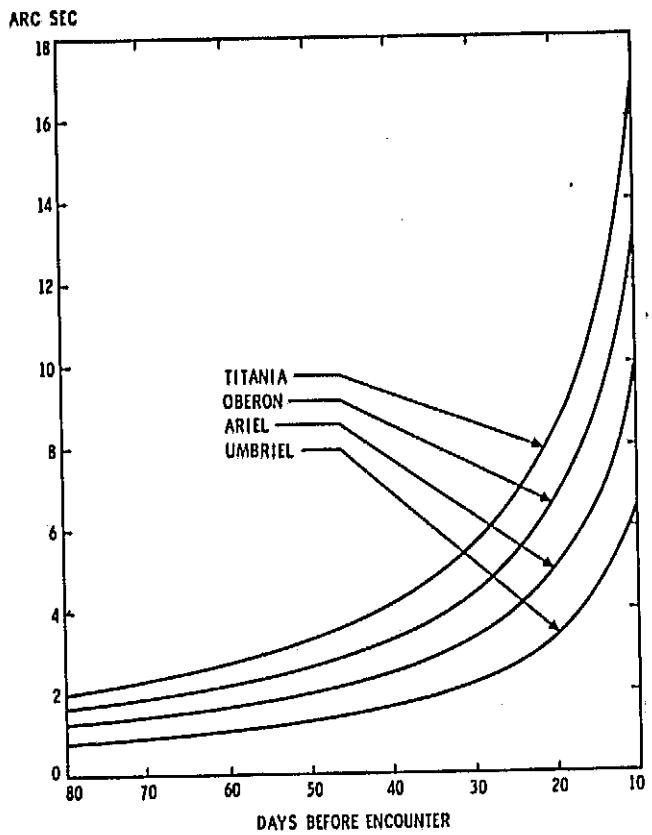

Fig. 16. Saturn-Uranus Mission, Uranus Approach; Satellite Angular Diameter

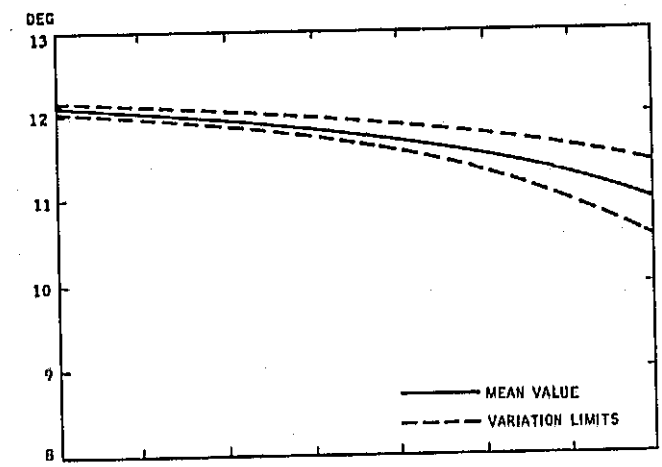

Fig. 17. Saturn-Uranus Mission, Uranus Approach; Satellite Phase Angle

cone angle required for the Saturn-Uranus mission.) The 7 deg narrow viewing cone angle is quite unfavorable for making approach guidance measurements with a V-slit scanner.

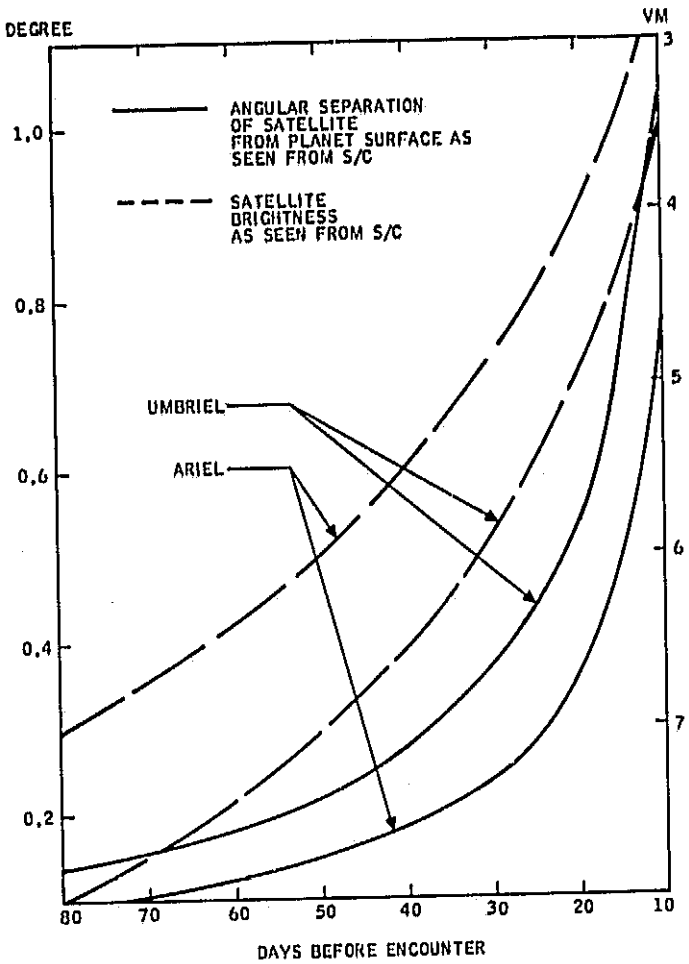

Fig. 18. Saturn-Uranus Mission, Uranus Approach; Satellite Viewing Parameters

The scanned star background with stars down to 4 and 5 VM is shown in Figs. 27 and 28, respectively. The figures also show the path of the spin axis pointing in the time period between E-80 and E-10 days. The apparent orbit of Titania from E-25 to E-16 day is also shown in the figures together with the apparent location of Uranus. The 3 deg wide annular scan of the V-slit sensor shown in Figs. 27 and 28 is centered at the spin axis pointing at E-20 day with coordinates $\delta = -23.28$ deg and $\alpha = 261.15$ deg; the cone angle is $\phi = 7.7$ and 4.7. The apparent location of Titania at E-20 day is also shown in the figures. The construction of the distorted small circles in a Cartesian frame has been explained previously.

As seen in Fig. 27, the 3 deg wide annular strip does not contain any star brighter than 4 VM. But there will be 3 stars with brightness between 4 and 5 VM within the scanned annular strip as seen in Fig. 28. It is worth noting that the total 25 deg by 25 deg celestial background contains only 6 stars brighter than 4 VM, or 21 stars brighter than 5 VM.

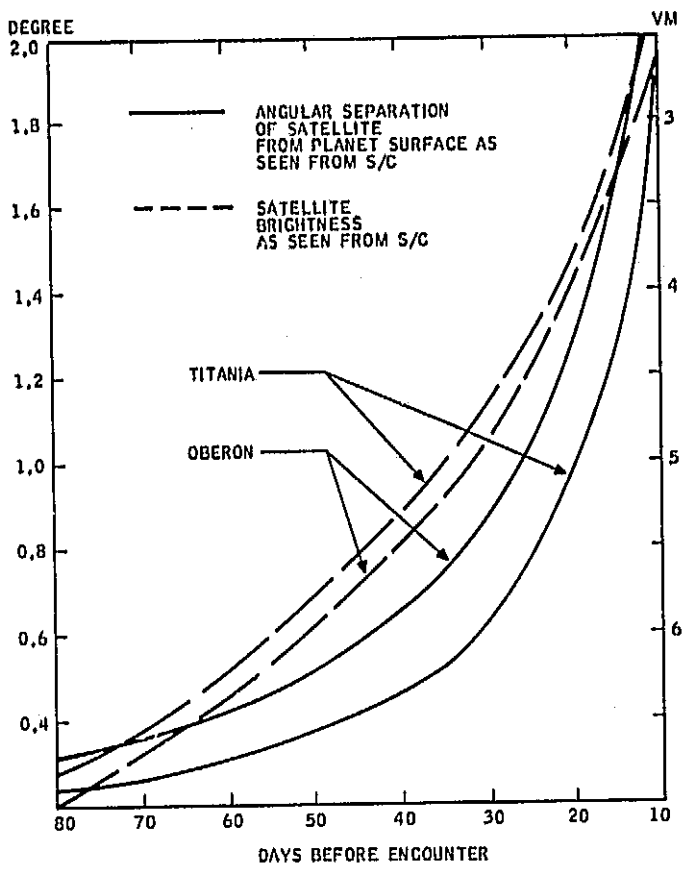

Fig. 19. Saturn-Uranus Mission, Uranus Approach; Satellite Viewing Parameters

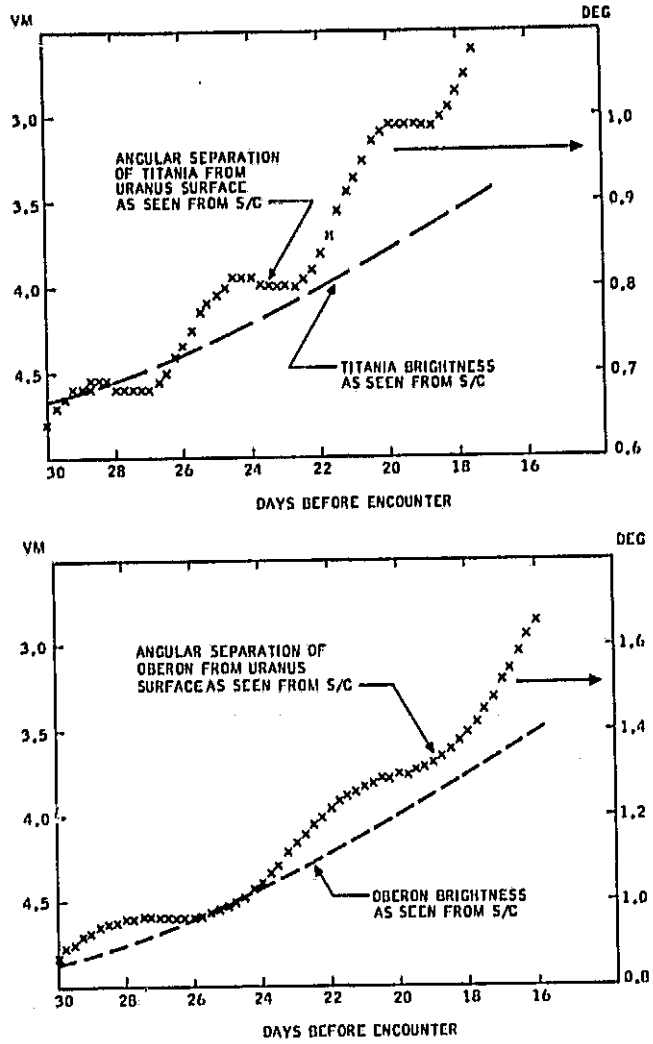

Fig. 20. Saturn-Uranus Mission, Uranus Approach; Satellite Viewing Parameters

VI. Spacecraft Attitude and Approach Guidance Measurements

The V-slit star mapper is a completely passive, strapped-down measuring device. Since the information to be obtained from the scanning V-slit sensor for approach guidance is spacecraft/satellite direction in celestial coordinates, the basic reference for obtaining the desired information is the spin axis orientation in celestial coordinates during the time when spacecraft-satellite measurements are taken against the detectable star background. Thus, to obtain precision information about the spacecraft-satellite direction in celestial coordinates requires a precision determination of the spin axis orientation in celestial coordinates. In general, therefore, the information accuracy requirements have an influence not only on the measurement accuracy required from the electro-optical system (that is, on the accuracy in the resolution of time detection of a star pulse), but also on the type of dynamical model for the attitude motion of the spacecraft utilized for determining the spin axis orientation.

Multislit star mapper onboard a spin-stabilized spacecraft has been successfully applied for attitude determination of several earth-orbiting satellites, as for instance, the OSO-7, ATS-III, and Project Scanner satellites. (Refs. 10, 13, and 14.) Experience shows (see the just quoted references) that the accuracy of the attitude solutions depends on two major factors: a) the selected

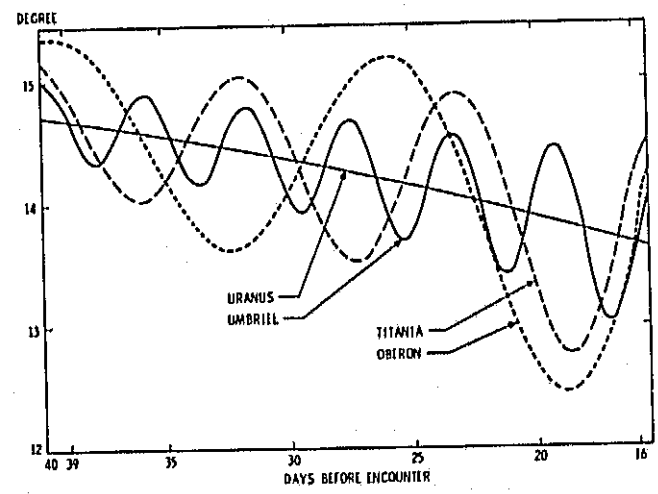

Fig. 21. Saturn-Uranus Mission, Uranus Approach; Satellite Viewing Cone Angle

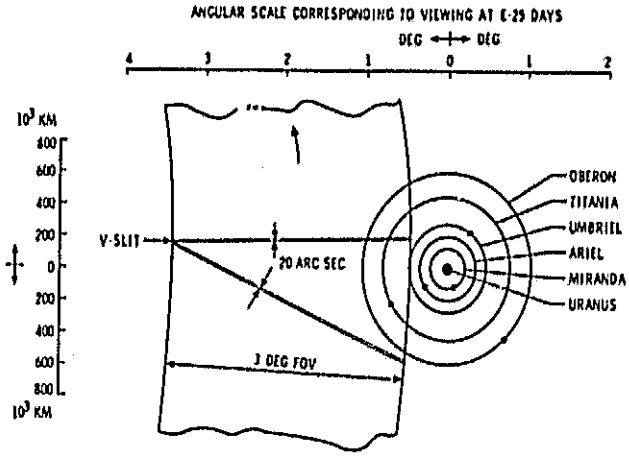

Fig. 22. Saturn-Uranus Mission, Uranus Approach; Satellite Viewing Geometry

dynamical model for the attitude motion, and b) good target geometry. (The importance of these factors is expected for theoretical reasons.) For instance, for the ATS III satellite, poor target geometry provided only 1.5 arc-min accuracy in the spin axis solution, while a good target geometry provided RSS three axis attitude errors in the range from 12 to 20 arc-sec. Target geometry means the distribution of stars within the scanned annulus. For instance, if all stars in a spin period are placed within half a period in the scanned annulus, then the precession is poorly defined. Further, in the case of the OSO-7 satellite, a simple inertially-fixed spin axis model provided an attitude solution accurate to 0.01-0.05 deg (1 σ error). But accounting for the nutation and wobble of the spacecraft, the approximate error per data sample could be reduced to about 20 arc-sec. Accounting for the nutation and wobble of the spacecraft means examining and evaluating the fine structure of the residuals of the reduced data.

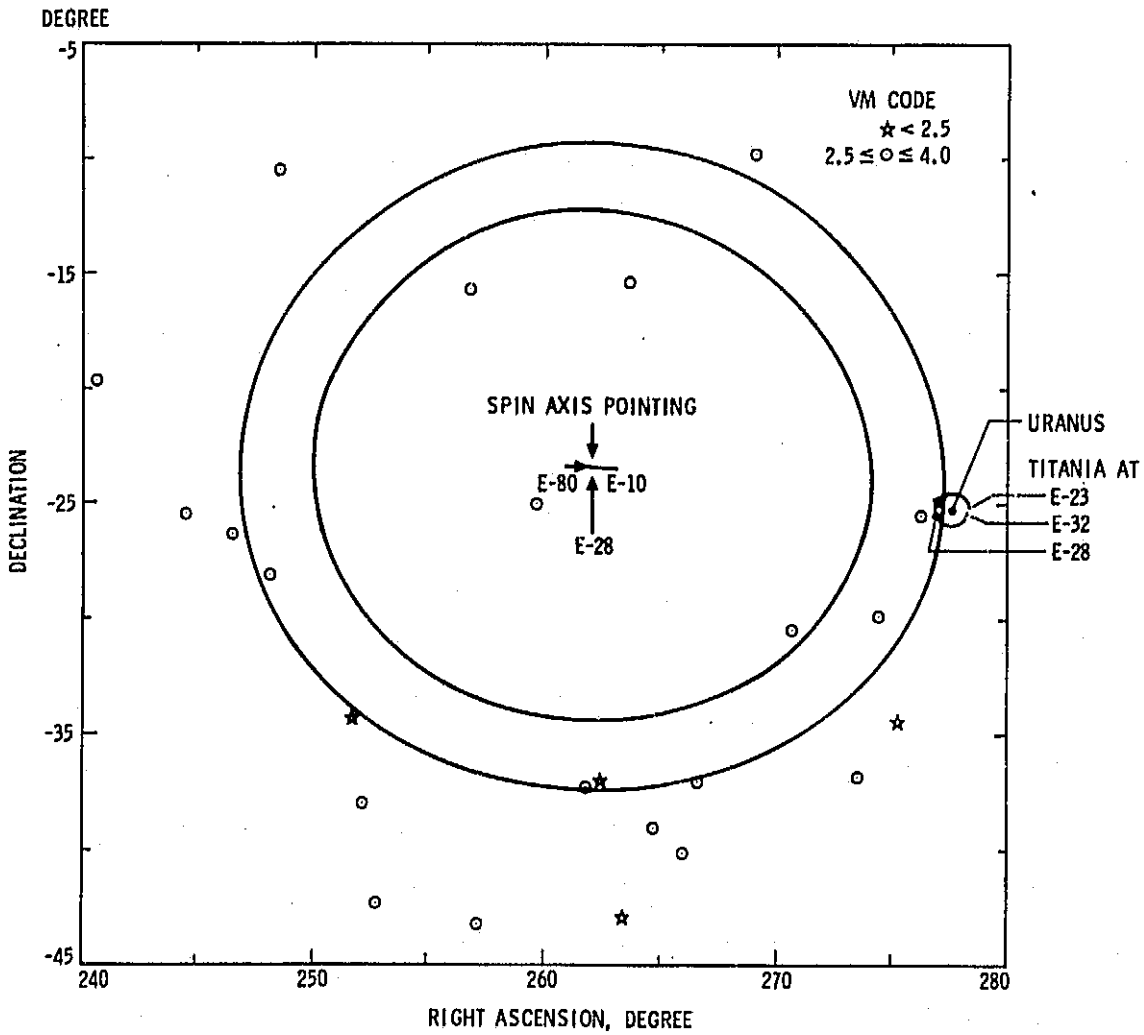

Fig. 23. Saturn-Uranus Mission, Uranus Approach; Tracking Titania Against Star Background, VM < 4

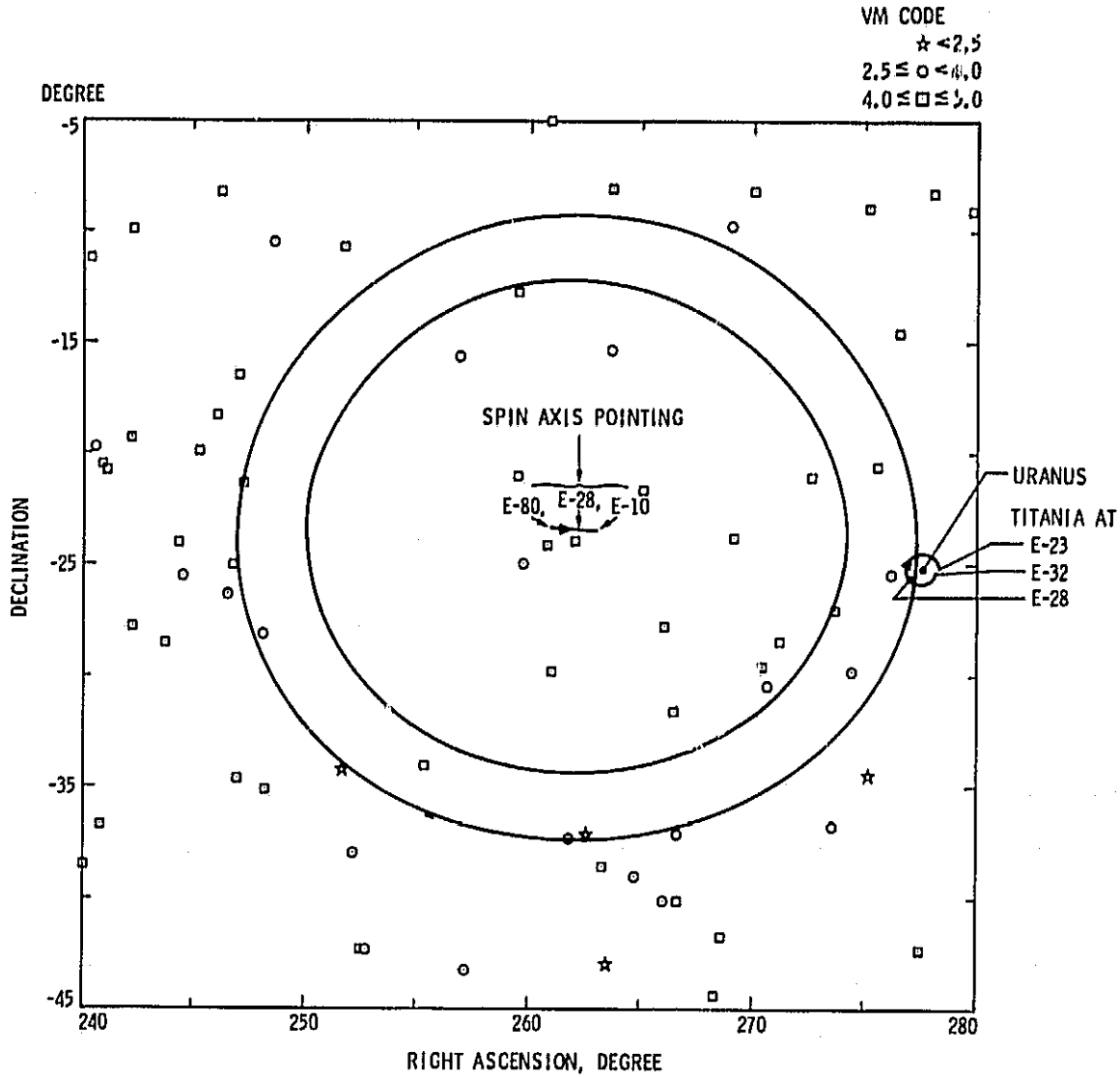

Fig. 24. Saturn-Uranus Mission, Uranus Approach; Tracking Titania Against Star Background; VM < 5

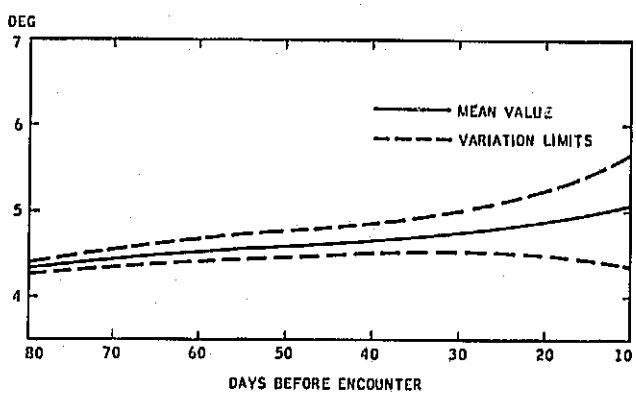

Fig. 25. Jupiter-Uranus Mission, Uranus Approach; Satellite Phase Angle

The data accuracy required for approach guidance measurements is in the order of 10^{-3} deg (≈ 5-10 arc-seconds). Keeping this in mind together with the flight experiences quoted above, it is seen that attitude motion modeling is an all-important factor to obtain precision approach guidance data by a V-slit sensor.

The requirement for spin axis pointing accuracy for the presently operational Pioneer 10 and 11 spacecrafts is 0.3-0.5 deg. The basic spin axis determination technique for Pioneer 10 and 11 is the CONSCAN. (Ref. 19.) The best accuracy obtainable by the CONSCAN technique is 0.1 to 0.2 deg.* Attempts have been made to verify the CONSCAN data by employing the Imaging Photo-polarimeter on Pioneer 10 in the imaging mode, (which has a narrow field of view, 0.03 deg) to observe stars, and using the celestial coordinates of the identified stars to obtain a solution for the

*G. Schimmel, NASA/Ames, private communication

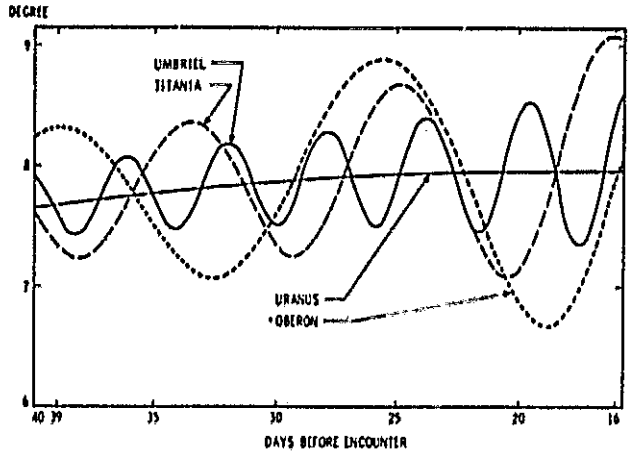

Fig. 26. Jupiter-Uranus Mission, Uranus Approach; Satellite Viewing Cone Angle

spin axis orientation by spherical triangulation. The solution obtained was within 0.07 deg of the spin axis orientation determined by the CONSCAN technique.*

To obtain experimental data for spin axis stability of Pioneer-type spacecrafts at the 0.01 deg or lower resolution level, flight measurements were proposed and recently performed on Pioneer 10 by using the Imaging Photopolarimeter locked on Jupiter for an extended period of time. (8 and 28 hours). The measurements are described in some detail in the Appendix at the end of this paper.

VII. Discussion of Results

As seen in Section V the V-slit star mapper must deal with two distinctly different satellite viewing parameters at Saturn and Uranus. If we select Titan and Rhea at Satu' 1 and Titania

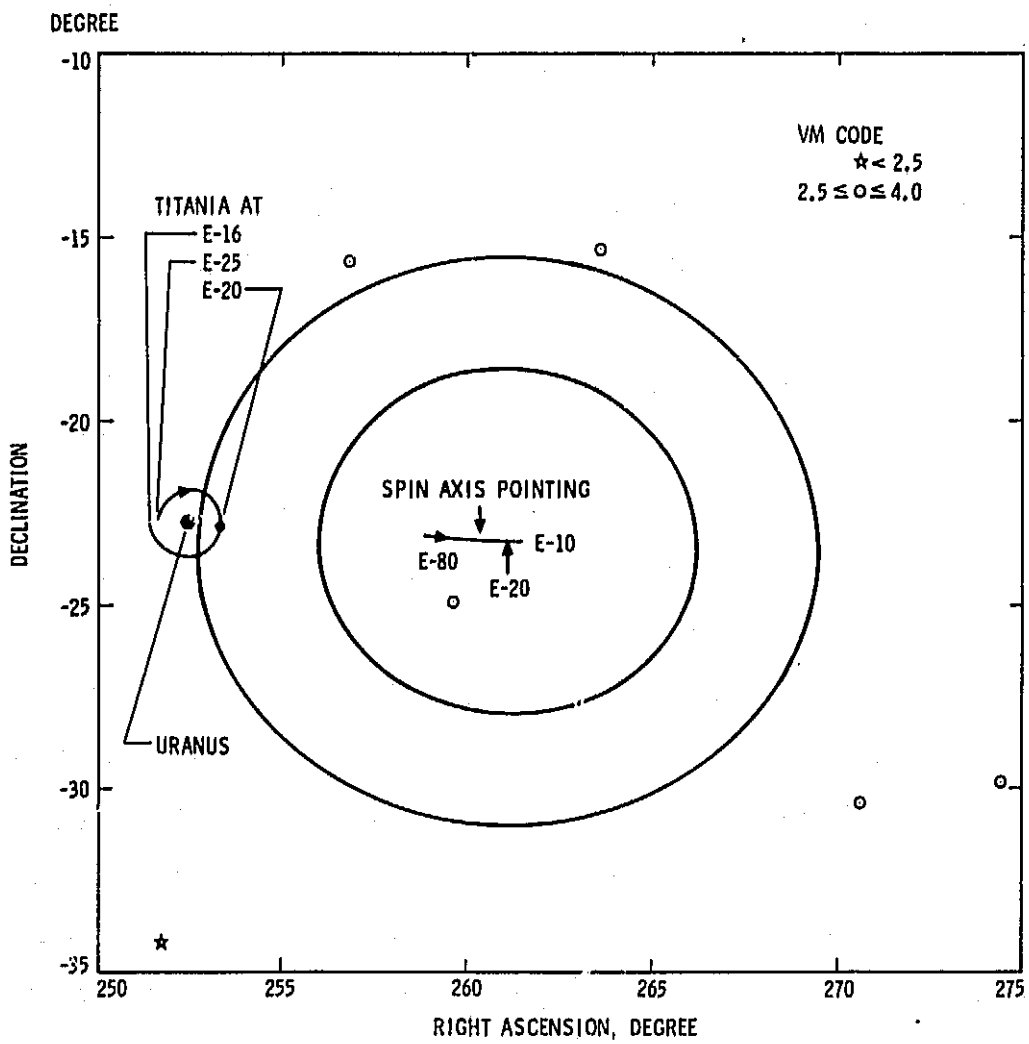

Fig. 27. Jupiter-Uranus Mission, Uranus Approach; Tracking Titania Against Star Background, VM < 4

*L. Doose, University of Arizona, Tucson, Az, private communication

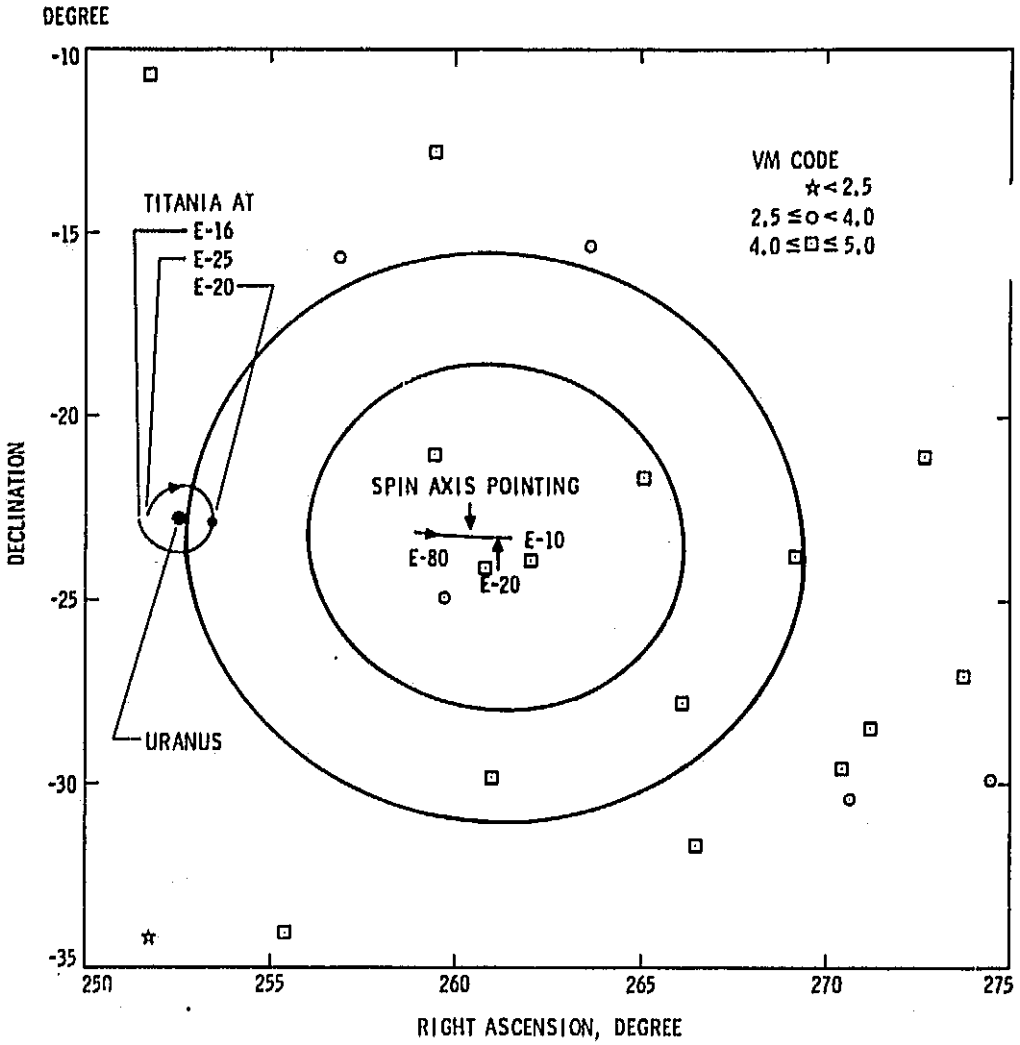

Fig. 28. Jupiter-Uranus Mission, Uranus Approach; Tracking Titania Against Star Background, VM < 5

and Oberon at Uranus as targets for approach guidance measurements, then the difference can be summarized as follows:

1. The two target satellites at Saturn are brighter than the two target satellites at Uranus by 1.5 to 2.5 VM. Consequently, using a given sensitivity V-slit sensor (say 4 VM), the Saturn satellites can be detected much earlier than the Uranus satellites. The detection time difference amounts to several weeks flight time.

2. The orbital distance and period of the Saturn satellites provide more favorable measurement procedures than the orbital distance and period of the Uranus satellites.

3. The satellite viewing cone angle at Saturn flyby is much better than the satellite-viewing cone angle at Uranus approach. In fact, the satellite viewing cone angle at Uranus for the Jupiter-Uranus mission is extremely low (7 to 9 deg) which may render the V-slit sensor measurements quite difficult.

4. Viewing Titan constitutes a unique case due to the large body (radius) of Titan. While all other Saturn and Uranus satellites can be considered as true point objects (few arcsec angular diameter) at E-30 day, Titan's apparent angular diameters exceed 20 arc-sec already at E-50 day.

A 4 VM sensitivity V-slit star mapper would be sufficient for approach guidance measurements at Saturn. However, a 5 VM sensitivity V-slit star mapper would be required for a safe approach guidance measurement performance at Uranus.

Regarding stray light interference, there are no established bounds on the minimum apparent angular separation of the observed object from the planet surface when a V-slit sensor is used for approach guidance measurements. As pointed out in Section V, the requirement to observe the Uranus satellites at earlier preencounter days by using a higher sensitivity V-slit sensor will inevitably lead to a very narrow observation geometry which may decrease the signal to noise ratio below the critical level.

Two alternative ideas can be suggested which could ease the approach guidance measurement problem at Uranus using a V-slit sensor.

1. If possible, change the probe-bus separation day from E-20 day to E-15, or preferably to E-10 day. Examining Figs. 16 through 20, it is seen that the brightness and geometry conditions for satellite viewing are considerably better during the time period from E-20 to E-10 days as compared to the conditions during the time period from E-35 to E-20 days.

2. Instead of the satellites, Uranus itself could be the object for V-slit sensor approach guidance measurements. As seen in Figs. 14 and 15, Uranus is brighter than minus 1.5 VM and its angular diameter is between 100-200 arc-sec as seen from the spacecraft during the time period from E-60 to E-40 days. If the planet center could be determined, for instance, within 8 arc-sec accuracy during this time period using V-slit sensor measurements, then a rough estimate shows that the presently predicted 10^4 Km navigation error at Uranus could be reduced by a factor of 5. Regarding Uranus tracking by a V-slit sensor, several possible instrumentation and data evaluation techniques could be explored. It may even be feasible to track Uranus by a V-slit sensor at a closer approach (say, in the time period from E-30 to E-10 days) and obtain considerable reduction in the delivery error. An improved Imaging Photopolarimeter combined with a V-slit reticle (as discussed in Ref. 9) may also be applicable for Uranus tracking against the star background to reduce terminal navigation error.

Tracking Uranus implies the sensing of an extended body by the V-slit star mapper. The implications of extended body sensing by a V-slit star mapper is beyond the scope of this paper. However, as pointed out previously, sensing Titan at Saturn approach already implies the sensing of a nonpoint, extended object. Titan is a prime target candidate for approach guidance measurements at Saturn approach. Thus, the investigation of extended body sensing by a V-slit star mapper serves a more general interest.

Acknowledgment

The cooperation of R. H. Stanton and W. G. Breckenridge of JPL in providing computer programs employed in this study is gratefully acknowledged. The flight measurements on Pioneer 10 were carried out with the generous cooperation of the Pioneer Project Office, the University of Arizona IPP Team, and the Deep Space Network Scheduling Team. The Pioneer Trajectory Group at JPL provided some of the data required for measurement interpretation.

References

1. "Outer Solar System Exploration — An Overview", Space Sciences Reviews, Vol. 14, Nos. 3/4, March/May 1973.

2. Swenson, B. L., Tindle, E. L., Manning, L. A., Mission Planning for Pioneer Saturn/Uranus Atmospheric Probe Missions, NASA TM-X-2824, Ames Research Center, Moffett Field, Calif., September 1973.

3. Park, R. A., Jenkin, K. R., Layton, D. M., Terminal Guidance Sensing From A Spinning Spacecraft, AAS 17th Annual Meeting, Seattle, Washington, Conference Preprint No. AAS-71-121, June 28-30, 1971.

4. Study of Multiple Asteroid Flyby Missions, Final TRW Report for NASA/Ames, Contract No. NAS2-6866, November 17, 1972.

5. Saturn-Uranus Atmospheric Entry Probe Mission Spacecraft System Definition Study, Final TRW Report for NASA/Ames, Contract No. NAS2-7297, July 15, 1973.

6. Paul, C. K., Russell, R. K., Ellis, J., Advanced Pioneer Guidance and Navigation Requirements for Outer Planet Missions, Conference Paper, AAS/AIAA Astrodynamics Conference, Vail, Colorado, July 16-18, 1973.

7. Duxbury, T. C., Born, G. H., Jerath, N., Viewing Phobos and Deimos for Navigating Mariner 9, Conference Paper, AIAA/AAS Astrodynamics Conference, Palo Alto, California, September 11-12, AIAA Paper No. 72-927.

8. Acton, C. H., Jr., Processing Onboard Optical Data for Planetary Approach Navigation, Conference Paper, AIAA 10th Aerospace Sciences Meeting, San Diego, California, January 17-19, 1972, AIAA Paper No. 72-53.

9. Feasibility of Using the Pioneer 10/11 Imaging Photopolarimeter as Navigation Sensor in Future Pioneer Missions, TRW Study Report for Ames, Contract No. NAS2-6859, December 20, 1973.

10. Mackinson, D. L., Gutshall, R. L., Volpe, F., Star Scanner Attitude Determination for the OSO-7 Spacecraft, Journal of Spacecrafts and Rockets, Vol. 10, No. 4, p 262, April 1973.

11. Breckenridge, W. G., and Duxbury, T. C., "Investigation of Planetary Navigation Using Spacecraft-Based Measurements," Proceedings of the Institute of Navigation National Space Meeting on Space Navigation — Present and Future, Institute of Navigation, 1969, pp. 18-30.

12. Duxbury, T. C., "A Spacecraft-Based Navigation Instrument for Outer Planet Missions," AIAA/AAS Astrodynamics Conference, Princeton, N.J., August 20-22, 1969, Paper No. 69-902.

13. Grosch, C. B., LaBonte, A. E., Vanelli, B. D., "The SCNC Attitude Determination Experiment on ATS-III," Proceedings of the Symposium on Spacecraft Attitude Determination, The Aerospace Corp., El Segundo, Calif., October 1969.

14. Walsh, T. M., Hinton, D. E., "Development and Application of a Star-Mapping Technique to Attitude Determination of the Spin-Stabilized Project Scanner Spacecraft," Proceedings of the Symposium on Spacecraft Attitude Determination, The Aerospace Corp., El Segundo, Calif., October 1969.

15. Gates, R. F., Flannery, J. V., Cragin, J. T., Feasibility Test for a V-Slit Star Mapper for Pioneer Spacecraft Terminal Navigation, Final TRW Report for NASA/ Ames Contract No. NAS2-7597, November 1973.

16. Allen, C. W., Astrophysical Quantities, University of London, The Athlone Press, 1963.

17. Explanatory Supplement to the Astronomical Ephemeris and the American Ephemeris and Nautical Almanac, Atlantic House, Holborn Viaduct, London, England, E.C.I.

18. Newburn, R. L., Jr., Gulkis, S., A Brief Survey of the Outer Planets Jupiter, Saturn, Uranus, Neptune, Pluto and Their Satellites, JPL TR 32-1529, April 15, 1971.

19. Pioneer Program, Spacecraft Characteristics and Operation Book, NASA Ames Research Center, Moffett Field, Calif., 1971.

20. L.A. Watts, Pioneer F/G Imaging Photopolarimeter Instrument (IPP), Final Technical Report, Santa Barbara Research Center, August 10, 1973.

APPENDIX

MEASUREMENT OF LONG TERM SPIN AXIS STABILITY OF PIONEER 10

To obtain 20 arcsec or better approach guidance measurement accuracy from a star/target map generated by a V-slit sensor strapped down to a spinning spacecraft, it is required to know about the spin axis behavior of the spacecraft on a 20 arcsec or better resolution level.

An optical measurement experiment was recently defined and carried out on Pioneer 10 to investigate the long term stability of the spacecraft spin axis at a 20 arcsec resolution level. This level of resolution is not obtainable from the standard CONSCAN attitude measurements. The optical measurements employed the onboard Imaging Photopolarimeter (IPP) in the imaging mode which has a 0.5 mrad (100 arcsec) square field of view. (A detailed description of the IPP can be found in Ref. 20.) The experiment was defined as follows.

> Consider the IPP locked on Jupiter in the imaging mode for an extended period of time when the apparent light-reflecting angular diameter of Jupiter is comparable to the 100 arcsec field of view of the sensor. The intensity variation of the integrated brightness signatures of Jupiter as recorded by the IPP would indicate changes in the apparent cone angle of Jupiter as seen from the spacecraft, while the shift of the brightness signatures in the roll sectors would indicate changes in the apparent clock angle of Jupiter as seen from the spacecraft and referenced to the Sun. Subtracting sensor noise and the relative natural motion of Jupiter in the cone and clock angle directions from the recorded intensity signatures, the residual variations would indicate small changes in the inertial orientation of the spacecraft spin axis during the same time period. The main point of the measurements is to detect small variations (less than 20 arcsec) in spin axis orientation and study the characteristics of the detectable variations.

Two measurement experiments were carried out. The first experiment on May 27-28, 1974 had the IPP pointing cone angle (look angle) locked on Jupiter nearly for 8 hours which provided about 2400 subsequent scannings of Jupiter. The second experiment was on June 18-19, 1974. This time, the IPP look angle was locked on Jupiter nearly for 28 hours which provided about 8400 subsequent scannings of Jupiter.

Fig. A-1 shows the viewing parameters of Jupiter relative to Pioneer 10 during April-September, 1974. As seen in Fig. A-1, the apparent size of the total Jupiter disk was about 210-200 arcsec during late May and mid June. But the phase angle of Jupiter during the same time period was about 110 degrees so that the illuminated part of the Jupiter disk (a crescent) was at most 90-95 arcsec wide in the cone angle direction. That is, Jupiter as seen from Pioneer 10 during late May and mid June was a 200-210 arcsec long and 90-95 arcsec wide bright object in the clock and cone angle directions, respectively. This means that the IPP with the 100 arcsec square aperture could sense Jupiter in three subsequent roll sectors and at two subsequent look angles each by 100 arcsec apart as shown in Fig. A-2. These predictions were clearly verified during the search process for Jupiter.

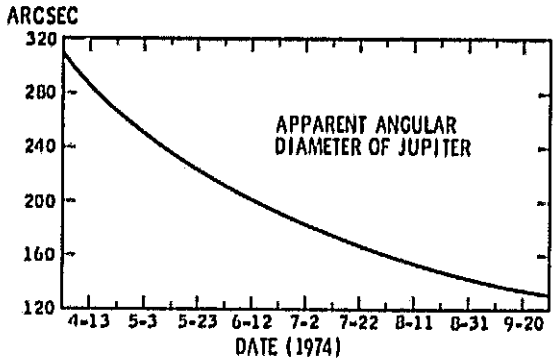

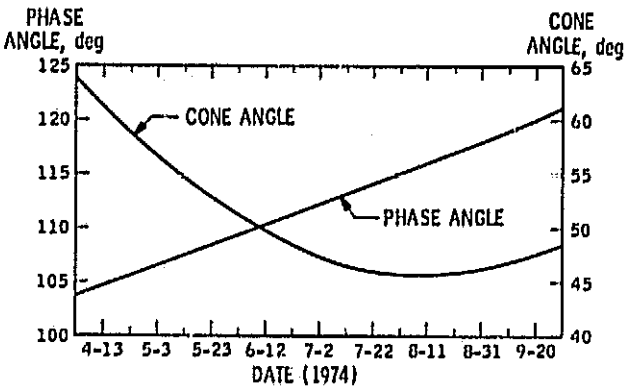

Fig. A-1. Jupiter Viewing Parameters Relative to Pioneer 10

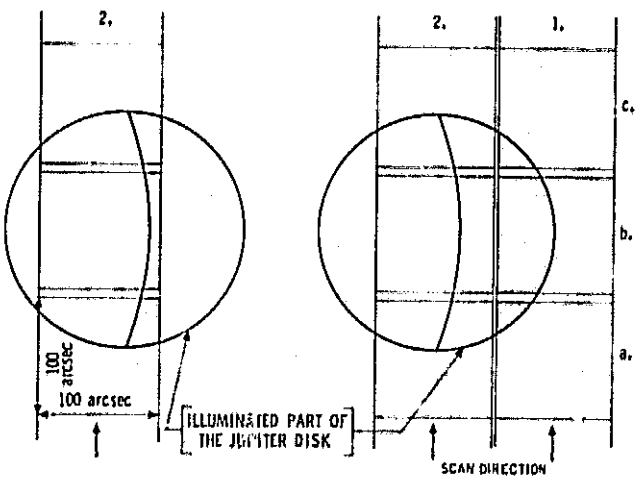

Fig. A-2. Scanning Jupiter from Pioneer 10 with the IPP in the Imaging Mode in May/June 1974

It is also seen in Fig. A-1 that the cone angle of Jupiter relative to Pioneer 10 was decreasing during late May and mid June. This means that, in the cone angle direction, Jupiter will move toward the Sun relative to a fixed IPP look angle as time goes on. Therefore, if the look angle position is initially selected so that the 100 arcsec field of view contains the dark limb side of the Jupiter disk (see look angle position no. 2 on the right part of Fig. A-2) then the 100 arcsec square aperture of the IPP locked on that look angle will cover less and less illuminated segments of the Jupiter disk as time goes on. (See look angle position no. 2 on the left part of Fig. A-2.) This measurement rationale was followed in the second experiment.

Fig. A-3 shows several sets of samples of the IPP intensity output from the second measurement experiment. Both the red and blue channel outputs are shown. (It is noted that the blue channel outputs contain considerable shot noise which is not subtracted from the displayed histograms. Typically, the values shown in the first and last roll sectors of the blue intensity histograms are nearly equal to the instrument noise.) The

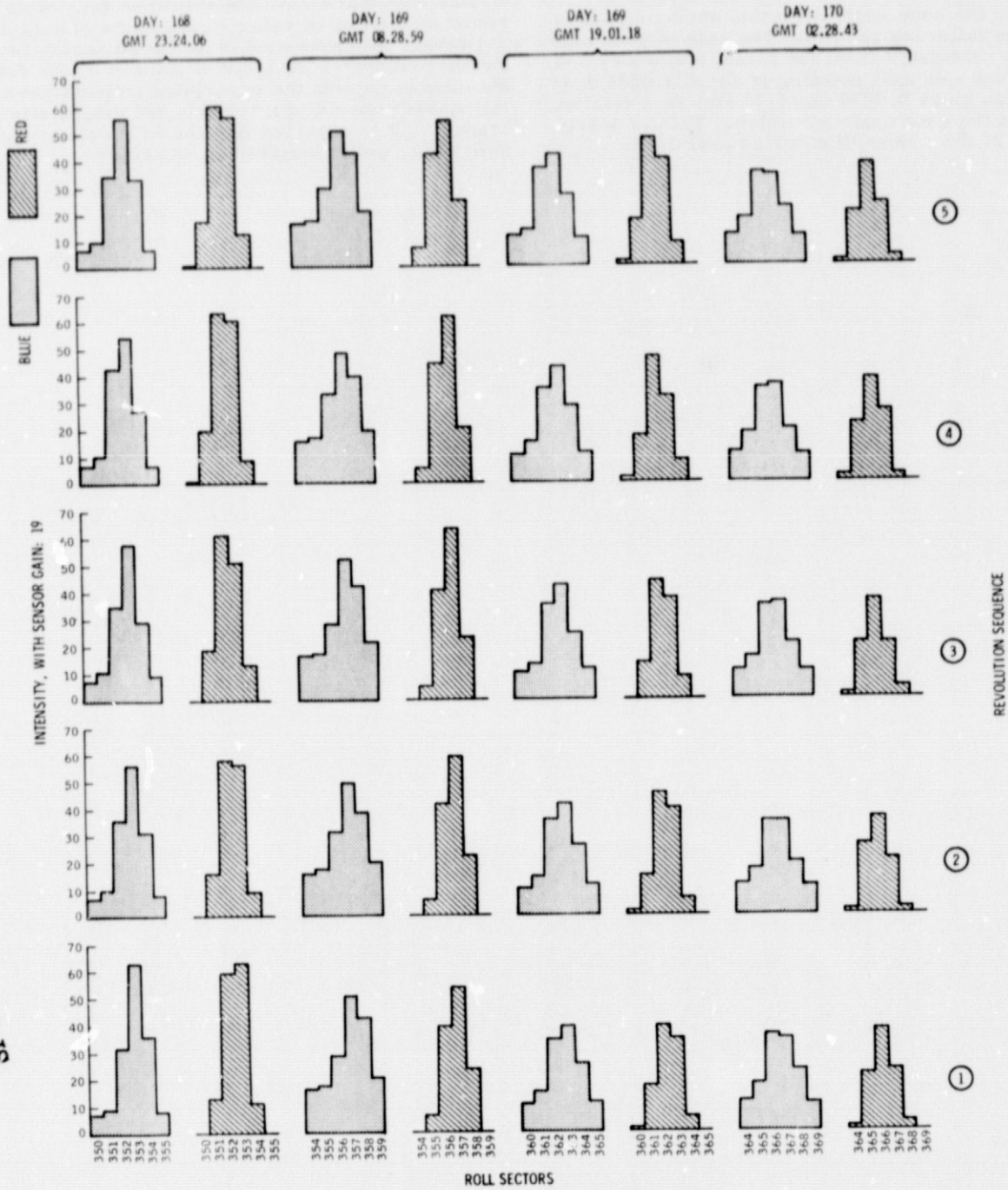

Fig. A-3. Scanning Jupiter in June 1974; Output Samples from the IPP in the Imaging Mode

It is also seen in Fig. A-1 that the cone angle of Jupiter relative to Pioneer 10 was decreasing during late May and mid June. This means that, in the cone angle direction, Jupiter will move toward the Sun relative to a fixed IPP look angle as time goes on. Therefore, if the look angle position is initially selected so that the 100 arcsec field of view contains the dark limb side of the Jupiter disk (see look angle position no. 2 on the right part of Fig. A-2) then the 100 arcsec square aperture of the IPP locked on that look angle will cover less and less illuminated segments of the Jupiter disk as time goes on. (See look angle position no. 2 on the left part of Fig. A-2.) This measurement rationale was followed in the second experiment.

Fig. A-3 shows several sets of samples of the IPP intensity output from the second measurement experiment. Both the red and blue channel outputs are shown. (It is noted that the blue channel outputs contain considerable shot noise which is not subtracted from the displayed histograms. Typically, the values shown in the first and last roll sectors of the blue intensity histograms are nearly equal to the instrument noise.) The

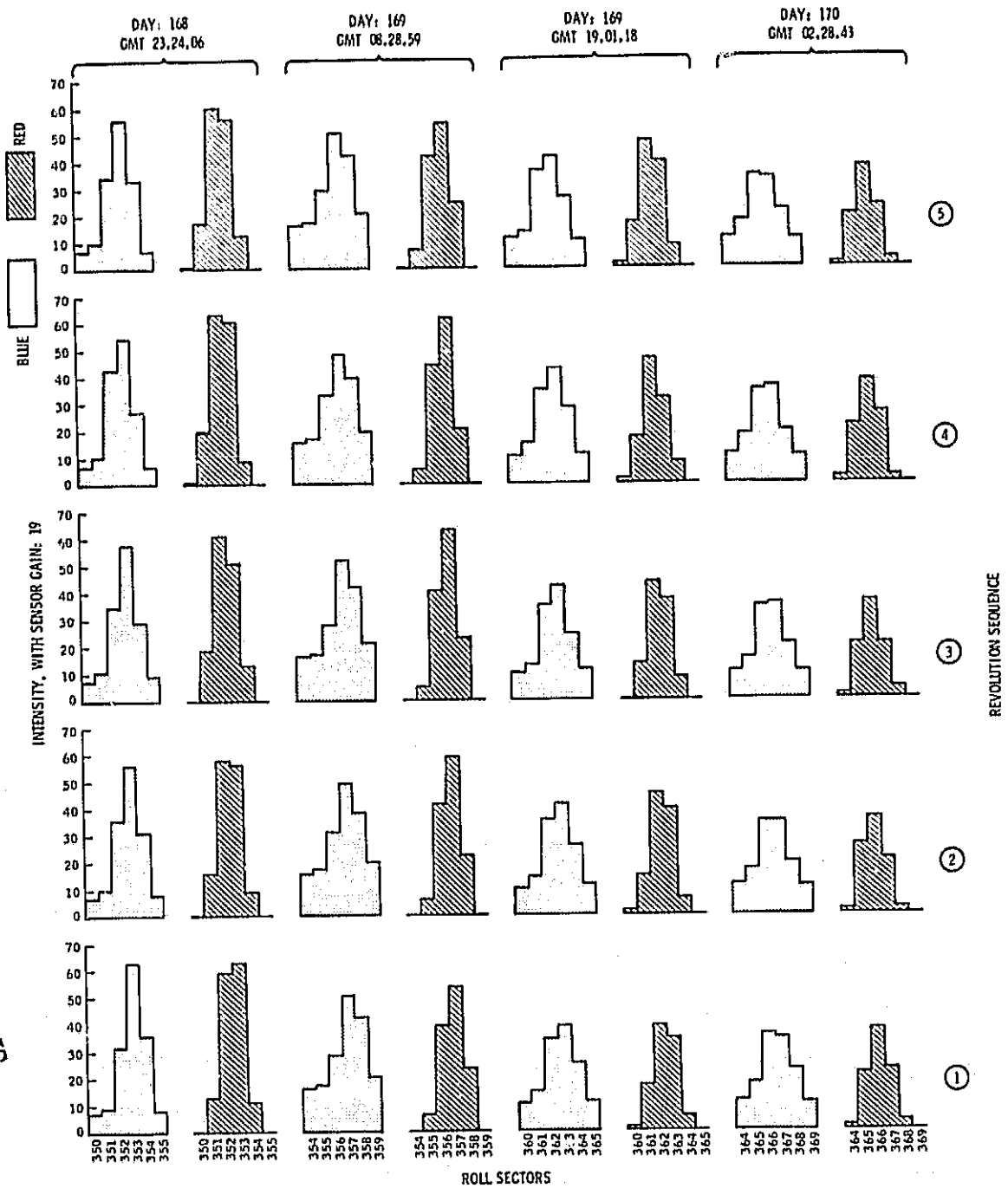

Fig. A-3. Scanning Jupiter in June 1974; Output Samples from the IPP in the Imaging Mode

bottom left histograms are among the first recorded data, and the upper right histograms are among the last recorded data. They are separated by about 27 hours. The time sequence of the histograms in each column starts at the bottom. Each column shows the IPP outputs in five subsequent revolutions covering 1 min time history per column. The time separation between the four columns can be seen from the Day/GMT time of data taking indicated at the top of the figure.

The overall decrease of the recorded intensity with time is clearly seen in Fig. A-3 as predicted. A rough calibration relating the change in the total light intensity to the relative natural motion of Jupiter in the cone angle direction during 27 hours shows the following results. The rate of cone angle decrease calculated from the actual trajectory and the nominal spin axis pointing is about 0.0002 deg/hour which gives 0.0054 deg (~20 arc-sec) relative motion in the cone angle direction. This is nearly one fifth of the widest illuminated part of the Jupiter disk in the cone angle direction. If the scanning cone angle in position no. 2 was initially so as indicated in the right part of Fig. A-2 (which agrees reasonably with the initial observations in positions 1 and 2) and if we move the cone angle by about 15-20 arcsec to the left (see the left part of Fig. A-2), it would produce about 50-60% decrease in the scanned illuminated part of the Jupiter disk which checks reasonably well with the observed value. Of course, this rough calibration only shows that position changes in the cone angle direction can be observed at least down to the 20 arcsec level. It does not mean that there is a spin axis wobble with that amplitude. It only means that wobble with that amplitude should be detectable. A visual evaluation of selected segments of data did not reveal spin axis wobble on the 20 arcsec level. Further computer analysis is planned on the data obtained to extract the underlying information from the measurements in a reliable and systematic manner. It is expected that the final data analysis will yield results better than 10 arcsec.

NASA — JPL — Coml., L.A., Calif.